Stellarator Simplification using Permanent Magnets (PM4Stell)

Final Scientific/Technical Report

Report No. PPPL-2023_215

March 28, 2023

WORK AUTHORIZATION NUMBER 19/CJ000/13/02

COOPERATIVE AGREEMENT NUMBER DE-AR0001264

LABORATORY Princeton Plasma Physics Laboratory

PRINCIPAL INVESTIGATORS Kenneth C. Hammond *(Jul. 2022 - present)*
David A. Gates *(Apr. 2020 - Jul. 2022)*

CO-PRINCIPAL INVESTIGATORS Robert Mercurio, SABR
David Maurer, Auburn University

PROJECT TEAM MEMBERS Douglas Bishop, PPPL
Arthur Brooks, PPPL
Amelia Chambliss, PPPL
Keith Corrigan, PPPL
Peter Dugan, PPPL
Robert Ellis, PPPL
Robert Lown, SABR
Craig Miller, Ansys
Djin Patch, Princeton University
Luke Perkins, PPPL
Adam Rutkowski, Princeton University
John Schmitt, Auburn University
Eric Stamper, Ansys
Dennis Steward, Ansys
Yuhu Zhai, PPPL
Caoxiang Zhu, PPPL

Abstract

This Report describes the design and prototyping of an array of rare-Earth permanent magnets to form a stellarator. This effort was motivated by the hypothesis that the usage of permanent magnets, rather than electromagnetic coils with complex geometry, could reduce the cost of stellarator construction and thereby make increase the feasibility of the stellarator as a technology for a fusion-based power plant. In this project, we have developed novel methods for specifying the positions, shapes, and polarizations of the magnets in the array, and have developed designs for mounting structures and tooling for assembly. We have also performed detailed finite-element modeling to qualify the accuracy of the magnetic field produced by the magnet array as designed, and to confirm that the structure can withstand the forces between the magnets. We have also developed techniques for measuring the magnetic field produced by the array once constructed, as well as for correcting errors in the field arising from misalignments and offsets within the tolerances for mounting and fabrication. Finally, we have constructed a tabletop prototype of a section of the array to qualify the concept for assembling and mounting magnets within the array.

Contents

Chapter 1

Executive Summary

This project, titled *Stellarator Simplification using Permanent Magnets* and abbreviated as "PM4Stell," sought to develop an innovative proposed technology with the promise of reducing the cost of a fusion reactor. The proposed technology, which had recently received significant attention in the scientific literature, entails the usage of permanent magnets to shape the confining field of a stellarator.

A *stellarator* is a doughnut-shaped device that confines a plasma with a strong magnetic field with the intent of enabling the plasma to reach sufficient temperatures and densities to undergo fusion reactions and thereby produce energy. For stellarators to work properly, their magnet fields must be carefully shaped to confine the plasma effectively and avoid excessive particle and energy losses. State-of-the-art stellarators attain this shaping by using non-planar, superconducting electromagnetic coils. The complex shapes and tight engineering tolerances required of these coils have been a major cost driver for stellarators.

Permanent magnets were proposed as an alternative approach for three-dimensional field shaping that could potentially reduce the cost of stellarator construction. Some studies showed that permanent magnets could generate adequante shaping fields, as long as they were used in tandem with coils that provided a toroidal component to the confining magnetic field. These toroidal-field (TF) coils need not be complicated in shape or even non-planar. In this context, we proposed the PM4Stell project to determine the feasibility of the concept by designing and constructing a prototype array of permanent magnets for a stellarator, and confirming the accuracy of the field through direct measurements. This project would thereby verify the feasibility of the concept and clarify its strengths and limitations.

The project made significant strides in pursuit of this objective:

- Two software codes were developed: MAGPIE, to assist the design of the magnet layout, and FAMUS to optimize the dipole moments of the magnets to produce the required magnetic field.
- A patent-pending optimization procedure was developed to utilize these two codes to specify the arrangement and polarizations of the magnets in a way that made fabrication feasible while upholding the stringent field accuracy required for plasma confinement.
- A detailed design was produced for a mounting structure to hold the magnets in place around the stellarator against magnetic and gravitational forces.
- The design for the magnet array and mounting structure was verified through high-fidelity finite-element modeling to produce an accurate magnetic field and to have sufficient structural integrity in the face of the anticipated loads.
- Prototypes for magnets and portions of the mounting structure were fabricated and assembled as a verification of the feasibility of the concepts.

- A concept for a second array of permanent magnets was developed for the correction of errors in the magnetic field arising from misalignments in construction and non-ideal magnet effects. The correction concept enabled looser engineering tolerances, thereby reducing costs and complexity.

The ultimate goal of the project as originally proposed was to construct an array of permanent magnets corresponding to *half-period* of the stellarator, which would ultimately be comprised of six of these assemblies. During the project period, however, the project needed to be descoped due to unforeseen cost increases leading to budget shortfalls. These extra costs were driven primarily by the rising price of rare-Earth permanent magnets. To close the budget gap, the project was initially descoped to produce a sub-assembly of the half period. Ultimately, the decision was made by ARPA-E to terminate the project without constructing a magnet array beyond the prototypes mentioned above.

While the project objectives of magnet array construction and verification of field accuracy through direct measurement were therefore unfulfilled, the accomplishments of the project have nonetheless substantially advanced the field. The development of a first-of-its-kind detailed engineering design for a mid-scale permanent magnet stellarator has bolstered the credibility of the concept. In addition, the optimization procedures, mounting concept, and design workflows developed for this project can be generalized and adapted for future improved designs, thereby reducing the cost of entry for future project teams seeking to improve on the design or adapt the concept to the reactor scale.

Chapter 2

Accomplishments relative to project objectives

The original proposal for PM4Stell included four main objectives:

1. Design the magnet system including magnet mass, shape, position, and direction of magnetization; the support structure; and the mounting tolerances
2. Procure and manufacture the component parts including the support structure and the magnets
3. Assemble the magnets and support structure
4. Measure the resulting field and verify that the tolerances have been met within specification

Of the four enumerated project objectives, only (1) was completed in full, culminating with the project's final design review (FDR) hosted at PPPL on January 14, 2022. Due to the cancellation of the project in July of 2022, the remaining objectives could only be pursued in part. In the remainder of this section, the accomplishments of the project team in pursuit of the objectives will be summarized.

2.1 Magnet system design

The central challenge of the design of the magnet array for PM4Stell was to arrive at a solution that could produce the required magnetic field for a given stellarator plasma with sufficient accuracy, while also being feasible to fabricate and assemble within a mounting structure that could handle the electromagnetic and gravitational loads arising from the magnets. To address this challenge, we assembled an interdisciplinary team of physicists and engineers, as well as magnet manufacturers from our industrial partner, SABR Enterprises, LLC. The design underwent multiple iterations as various concepts for the individual magnets and their mounting structure were considered and improved upon.

2.1.1 Magnet types

In the final design, only three unique types of magnets are employed. All are cubic in geometry with a side length of three centimeters. The only difference between the three types is in the orientation of their polarization. These three polarization orientations are illustrated in Fig. 2.1. Keeping the number of unique magnet types limited in quantity is advantageous as it allows for a greater degree of standardization in the magnet fabrication, thereby keeping the process simpler and costs lower. While only three types of magnets are used, it should also be noted that, when considering possible rotations of the magnets, the three types

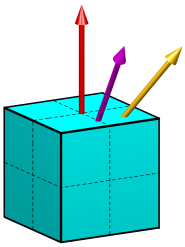

Figure 2.1: Orientations of the three polarization types used relative to the geometry of the magnets used in the design of the PM4Stell magnet array. The types are named as follows: red: face; magenta: face-edge; yellow: face-corner. Reproduced from [1].

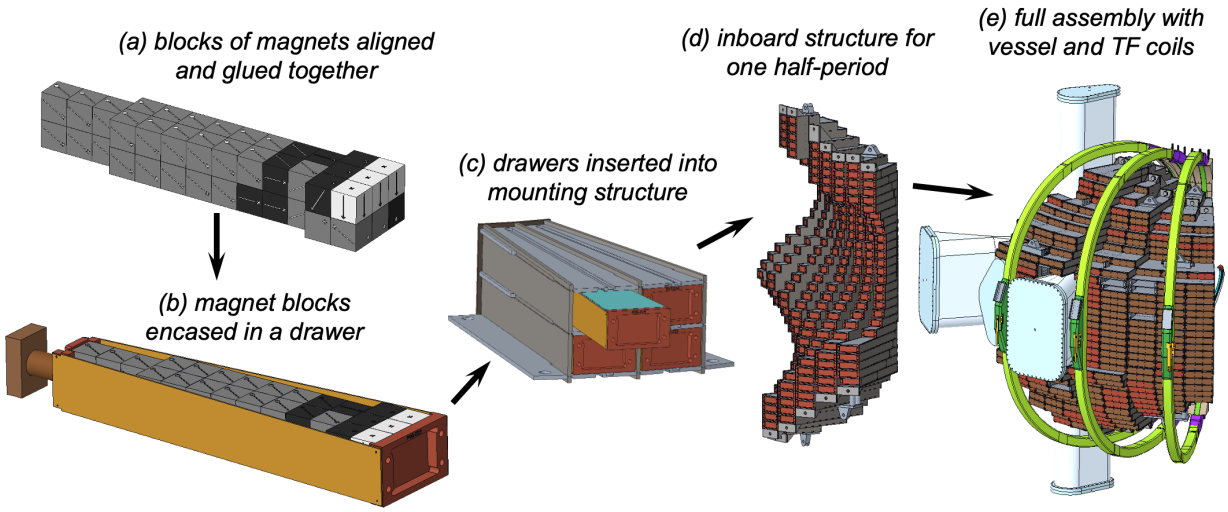

Figure 2.2: CAD renderings of the key components of the mounting scheme for the PM4Stell magnet array, along with descriptions of the steps in the assembly process. The markings on the individual magnets indicate the polarization vector direction, and the color (black, gray, or white) indicates the polarization type as shown in Fig. 2.1.

together can produce a total of 54 dipole moment vectors while maintaining the same geometric footprint. This flexibility is important for enabling a robust physics optimization, as described in Sec. 2.1.3. The 3 cm dimension was chosen to be the largest allowable by the fabrication process, which involves cutting magnets from slab of rare-Earth magnet material that is 5 cm thick and polarized perpendicular to the slab plane.

2.1.2 Mounting and assembly

The mounting structure for the magnets was designed to position the magnets as close to the plasma vessel as reasonably possible, as magnets positioned near the plasma boundary tend to provide the required magnetic field shaping more efficiently. At the same time, the structure needed to be feasible to construct and assemble and handle the forces arising from the magnets' fields and gravity. We ultimately arrived at the scheme illustrated in Fig. 2.2. The magnets in the array are to be grouped into *drawers* (Fig. 2.2a-b), which are inserted into a grid-like frame (Fig. 2.2c-d) that conforms closely to the geometry of the plasma vessel. The magnets and their mounting structure were designed to leave room for toroidal-field coils as well as access ports for plasma diagnostics and heating systems (Fig. 2.2e).

2.1.3 Determination of magnet positions and polarizations

The magnets in the array needed to be positioned and oriented to produce a three-dimensional magnetic field distribution with sufficient accuracy to confine the plasma equilibrium targeted for the experiment. Specification of stellarator magnets for a given plasma is typically accomplished with an optimization procedure, subject to constraints imposed by experimental boundary conditions. A special challenge posed by PM4Stell was the need for the solution to be within a discrete space, with the dipole moment of each magnet constrained to have one of the 54 polarization vectors permitted by the types depicted in Fig. 2.1.

To accomplish this task, we developed new procedures and new software to implement them. The MAGPIE code [2] was expanded to automatically generate arrangements of magnets compatible with the mounting and assembly scheme depicted in Fig. 2.2. The FAMUS code [3], derived from the FOCUS code [4], was developed to optimize the dipole moments of the individual magnets in the array subject to a constraint to prevent the moment magnitudes from exceeding the strength of rare-Earth magnets. The optimization procedure can be summarized as follows:

1. Generate an arrangement of cubic magnets
2. Perform a continuous optimization of the dipole moments of each magnet in two steps:
   (a) Minimize an objective function for magnetic field inaccuracy
   (b) Minimize a weighted sum of objective functions for field inaccuracy and intermediate dipole moment magnitudes
3. Rotate each optimized moment vector to the nearest allowable discrete vector

The outcome of this procedure for PM4Stell is shown in Fig. 2.3, which depicts the locations and polarization types of the magnets in the solution. Many of the magnets in the initial arrangement were determined to be unnecessary in the optimization procedure and are therefore omitted from this rendering. The gaps in the array left by these omitted magnets are to be filled with cubes of non-magnetic material during assembly. Overall, the solution consists of 35,436 magnets within a half-period, corresponding to a magnetized volume of 0.96 m^3. Extended to the full stellarator (six half-periods), this would require 212,626 magnets, or 5.74 m^3.

2.1.4 Scheme for error correction

It is anticipated that the magnet array will not produce exactly the field predicted by the optimizer. As is the case with all magnetically-confined plasma experiments, an *error field* will be present due to slight misalignments and offsets of the mounting structure, fabrication errors, and non-ideal properties of the magnets not accounted for in the optimization (discussed in more detail in Sec. 2.1.5). Since certain components of the error field can be deleterious to the plasma even in small magnitudes, it is important to have strategies for correcting error fields as they arise.

Present-day tokamaks and stellarators typically use dedicated sets of coils to correct error fields. For PM4Stell, we developed a novel correction concept in which a secondary array of permanent magnets, hereafter the *error-correcting* or EC array, is foreseen to be installed after the main magnet array is constructed and its error fields are measured [6]. Like the main magnets, the EC magnets have cubic geometry and one of the three polarization types shown in Fig. 2.1. Unlike the main magnets, however, the EC magnets are slightly smaller, with an edge length of 2 cm rather than 3 cm. As shown in Fig. 2.4a, the EC magnets are foreseen to be placed on the inside of the main magnet array, closer to the plasma boundary.

Once the main magnet array is constructed and its field is measured (Sec. 2.4), the required polarizations and locations for the error-correcting magnets can be determined using the essentially the same procedure

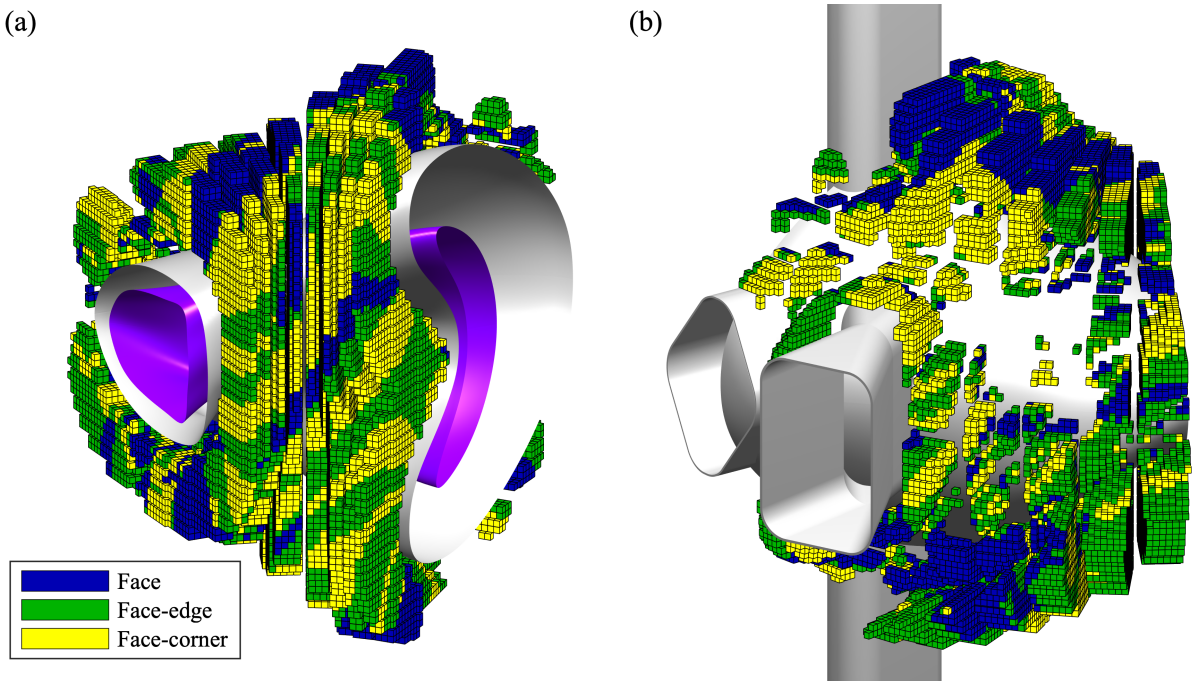

Figure 2.3: Positions of the magnets in one half-period of the solution for PM4Stell, color-coded according to the polarization types identified in Fig. 2.1. (a) inboard-side view, also showing the boundary of the target plasma equilibrium in magenta; (b) outboard-side view. Reproduced from [5].

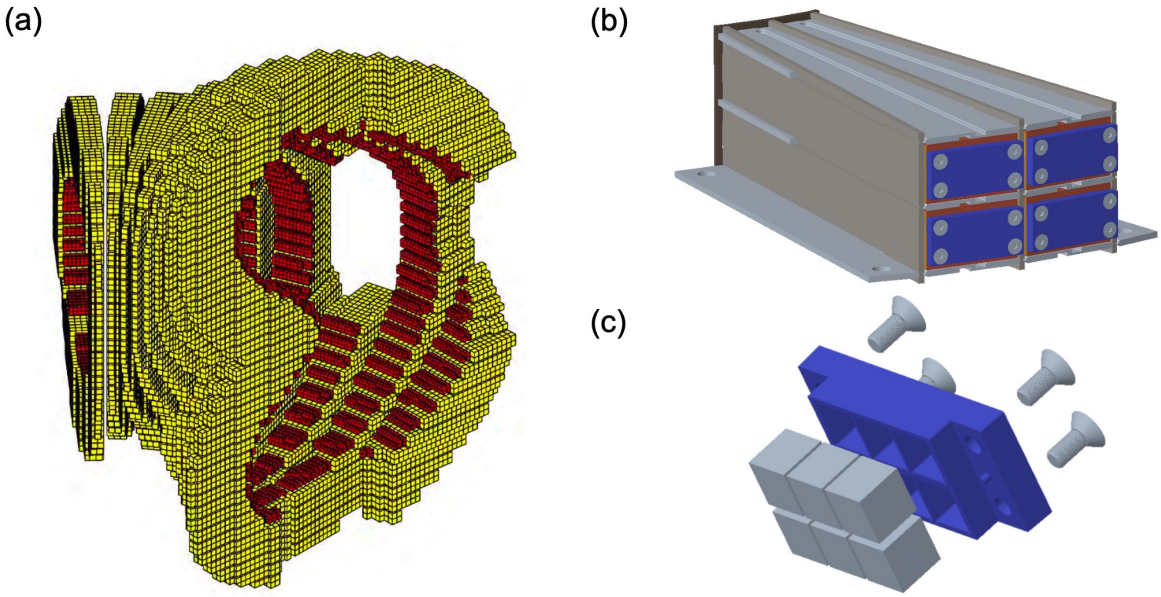

Figure 2.4: (a) Rendering of a sample magnet array for one half-period of a stellarator showing typical positions of EC magnets (red) relative to the main magnet array (yellow). (b) Concept for how the EC magnets (enclosed in the blue cases) can be mounted to the structure holding the main magnet array after it is constructed. (c) Exploded view of the EC magnets, a case, and screws used to fasten it to the main array.

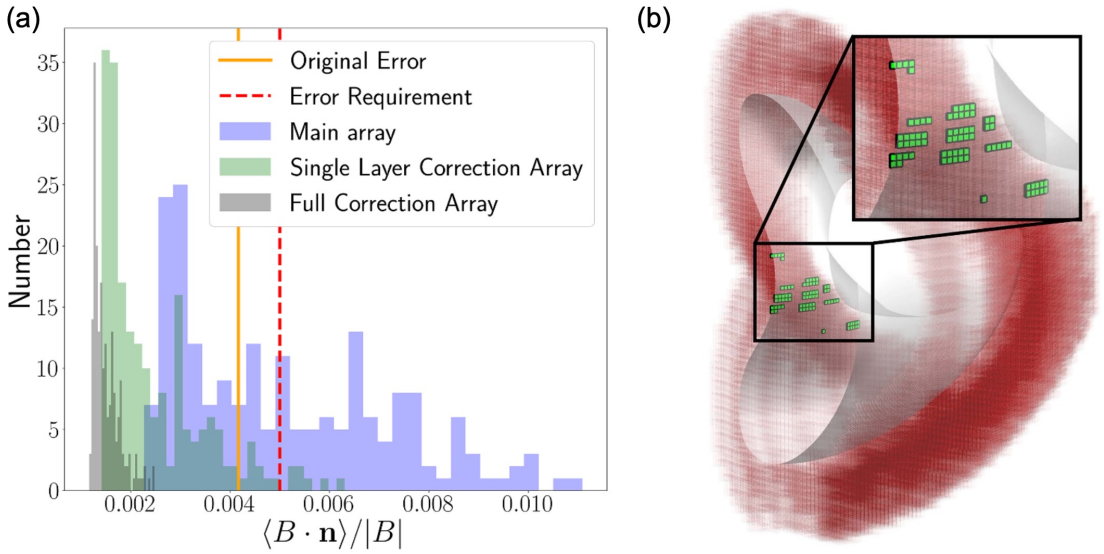

Figure 2.5: (a) Histograms illustrating the ability of the PM4Stell EC array to correct an ensemble of error fields arising from random geometric displacements and offsets in magnet properties. The red vertical dashed line represents the maximum allowable error field metric. The blue histogram represents the metric for the uncorrected fields from the ensemble of main arrays with randomized offsets. The green and gray histograms represent the error metric for fields corrected with a single layer of EC magnets and multiple layers of EC magnets, respectively. (b) Placement of a set of additional, thinner EC magnets determined to be sufficient for correcting a field error that resonates with the rational flux surface with rotational transform 3/5. Reproduced from [6].

used for the main magnet array as described in Sec. 2.1.3. In this case, the optimization objective function is determined by the error field requiring correction. Once the polarizations and locations are determined, the EC magnets can be mounted accordingly to the inside of the main magnet array in the casings illustrated in Fig. 2.4b-c.

To verify the effectiveness of this approach to error correction, an ensemble of simulated error fields was generated by calculating the field produced by the main magnet array subject to randomized perturbations. Perturbations were applied to the spatial positioning of individual magnets, as well as to portions of the mounting structure, with displacements within the engineering tolerances. In addition, random offsets were incorporated in the dipole moments of each magnet to simulate errors in fabrication. As shown in Fig. 2.5a, a single layer of EC magnets could correct the error fields from most of the simulated perturbed main arrays to below the criterion for field accuracy. If more than one layer of EC magnets is permitted, all simulated perturbed arrays could be corrected to well within the criterion.

Certain portions of the error field that resonate with rational magnetic flux surfaces within the plasma can be especially deleterious to plasma confinement. Our calculations have indicated that the plasma may be sensitive to these specific field errors in levels that are too small to be corrected by magnets with 2 cm cubic geometry. Hence, the possibility of using additional, thinner magnets to trim out these resonant fields has been investigated. A sensitivity analysis was performed to determine the portions of the main magnet array for which perturbations would most severely resonate with selected rational surfaces of the target plasma. Sets of thin magnets were placed in these locations and evaluated for their ability to trim out the corresponding resonant component of the error field. An example set of thin magnets is illustrated in Fig. 2.5b for trimming the field resonant with the rational surface with rotational transform 3/5. A sensitivity

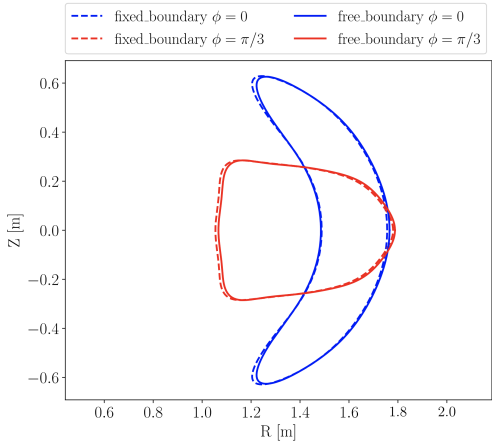

Figure 2.6: Comparison of cross-sections of the target plasma boundary (dashed lines) with the boundary of the plasma confined with the permanent magnets of the PM4Stell solution plus a set of TF coils (solid lines) at two toroidal angles ϕ. Reproduced from [1].

analysis has determined that these thin magnets can make sufficiently fine adjustments to the larger EC array for the purpose of reducing the resonant error fields.

2.1.5 Verification of the magnetic field with high-fidelity models

To build confidence in the design, it was important to perform high-fidelity calculations to verify the accuracy of its magnetic field. This accuracy verification entailed two main components. The first was to confirm that the magnetic dipole solution determined through the optimization procedure could indeed confine the target plasma equilibrium. This was verified through a free-boundary calculation with the VMEC magnetohydrodynamic (MHD) equilibrium code [7, 8]. One key output of this calculation is the shape of the boundary of the plasma that would form in the field created by the combination of permanent magnets and TF coils. A comparison of the actual plasma boundary with the target plasma boundary is shown in Fig. 2.6 and is considered sufficiently accurate.

To be tractable, the magnet optimization procedure and free-boundary modeling employed a simplifying approximation of the magnetic field in which each magnet in the array was treated as an ideal magnetic dipole and interactive effects between nearby magnets were neglected. It was therefore important to verify that the actual magnetic field produced by this solution was still sufficiently accurate when taking non-ideal effects into account. These effects included corrections to the dipole field near each magnet due to its finite dimensions, and absorption of field lines by the magnets due to the effects of (anisotropic) magnetic permeability.

For a high-fidelity calculation of the actual field from the magnet array, a finite-element model of the array was developed using the Ansys Maxwell software program. The model accounted individually for all 35,436 magnets in the half-period of the stellarator. Custom automation scripts were developed to construct the model in Ansys Maxwell according to the magnet specification. The model was developed with the assistance of representatives from Ansys, who were included in the project team. The complexity of the model motivated improvements to the Ansys Maxwell software base to reduce the processing time for the automated model construction procedure.

The Ansys Maxwell model was used to compute the magnetic field at test points on the boundary of the target plasma, accounting for the nonlinear B-H characteristics of each magnet as well as the potential for demagnetization in the ambient field. The magnets were assumed to have the B-H characteristic of NdFeB magnets of type N48M [9]. A typical comparison between the finite-element calculation and the idealized dipole approximation is shown in Fig. 2.7. While discrepencies between the idealized model and the finite element model are indeed observed as expected, the magnitude of the discrepancies is well within the range that is correctable with EC magnets. Therefore, it was concluded that the approach of using the dipole

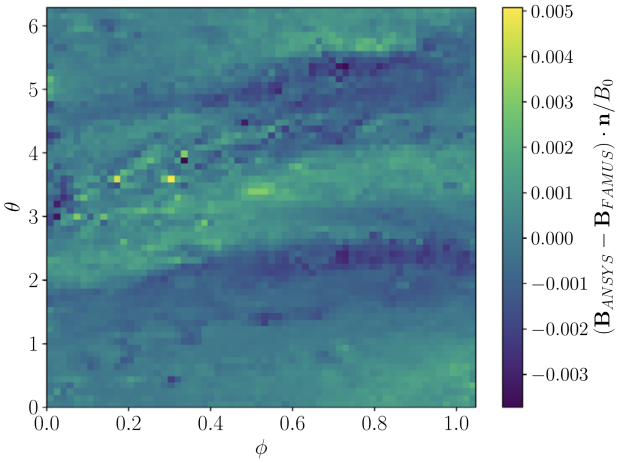

Figure 2.7: Difference in the normal component of magnetic field from one half-period of permanent magnets, calculated using the dipole approximation (B_{FAMUS}) and the finite element model (B_{Ansys}) from one on the boundary of the target plasma and normalized to the field on axis (0.5 T). The plasma boundary is parametrized according to toroidal angle ϕ and poloidal angle θ. Reproduced from [1].

approximation for magnet optimization was sufficient for realizing an accurate field with real magnets. This conclusion was further supported by supplementary calculations by the open-source MAGTENSE code [10, 11], which we used for calculations that included effects of finite magnet size and (linear) anisotropic permeability.

The same model was used to determine which magnets in the array were subject to demagnetization due to the ambient magnetic field. Demagnetization can occur if a permanent magnet is exposed to an external field above its *coercivity*, which is roughly 1 MA/m (equivalent to 1.3 T) at room temperature [9]. As shown in Fig. 2.8, demagnetization is expected to affect only a small minority of the magnets in the array.

2.1.6 Structural modeling

In light of the substantial forces expected between the neodynium magnets in the array, it was important to verify that the support structure would hold against these forces. To this end, we developed used the Ansys Mechanical software program to calculate the stresses and strains to be expected on the mounting structure.

As the PM4Stell array consists of blocks of magnets that are glued together and potted in epoxy, it was not necessary to determine the forces at the level of individual cubic magnets. Rather, to save computational expense, blocks of magnets within drawers (Sec. 2.1.2) were smeared together into monolithic bodies for the purposes of the model (Fig. 2.9a). Welds within the mounting structure were modeled as line elements. More detailed breakout models were also developed for some components considered especially sensitive, such as the joints used to fasten adjacent plate structures (Fig. 2.9b-c).

At the time of the final design review, a few isolated points of high stress had been identified in the design, including outboard weld joints, weldment spacer bolts, and the interface components between the inboard and outboard support structures. However, it was determined that these issues could be fixed with minimal alterations to the design.

2.2 Procurement and manufacture of component parts

Much of the procurement efforts undertaken in the project to date involved identification of potential suppliers for permanent magnets and qualification of their parts. Our industry partners at SABR performed a search for magnet suppliers who could fabricate cubic magnets with the polarization orientations specified in Fig. 2.1. Since the face-corner polarization type is non-standard, many magnet vendors offered no bid. However, three vendors were identified who were willing to supply parts to our specifications, and samples were ordered from each.

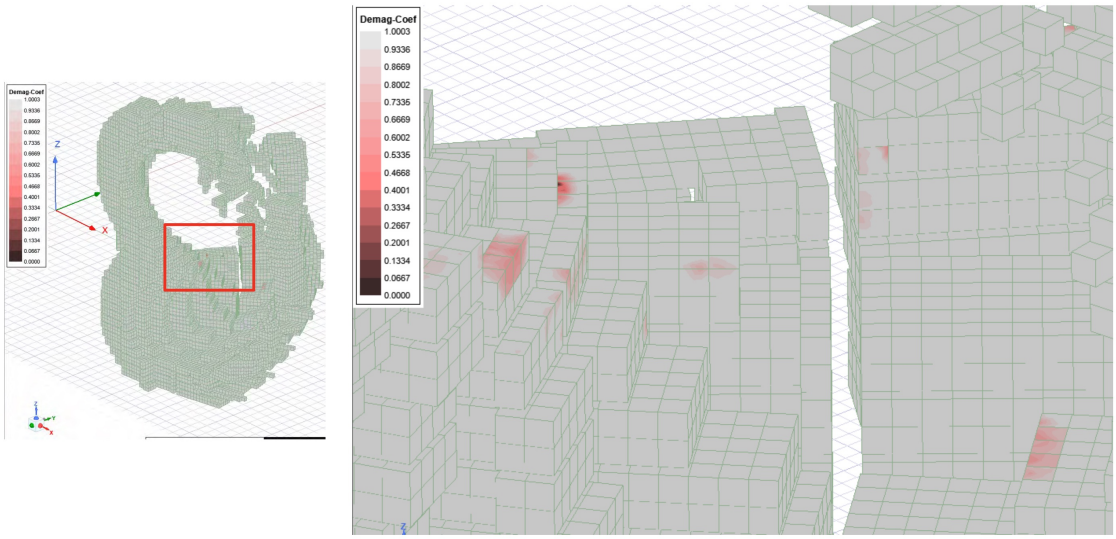

Figure 2.8: Demagnetization coefficients for the magnets in the PM4Stell half-period array. The ambient field in this calculation arises just from the half-period of magnets; additional fields, e.g. from TF coils, are not considered.

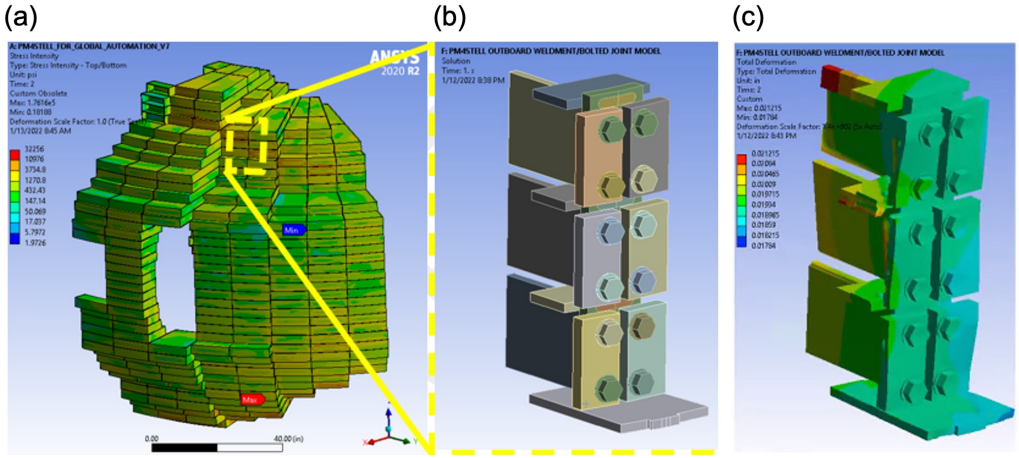

Figure 2.9: Results from mechanical modeling of the magnets and mounting structures: (a) view of the global model including smeared magnets for the full PM4Stell array, color-coded according to local stress intensity; (b) detailed breakout model for structures fastening adjacent components of the mounting structure; (c) exaggerated representation of the expected deformations to the fasteners in response to stresses.

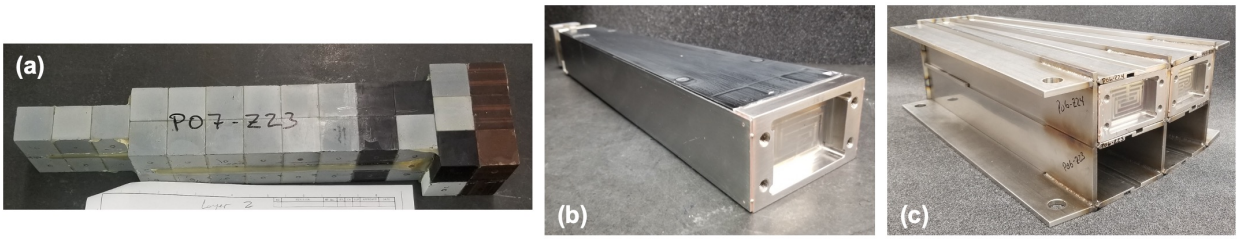

Figure 2.10: Photographs of the prototype assembly process: (a) a block of magnets and non-magnetized Garolite "blank" cubes glued together; (b) the magnet block potted and encased in steel to form a drawer; (c) two drawers inserted into the 2x2 frame.

To qualify the samples, it was necessary to measure their magnetic moments to confirm that the moment magnitude and orientation was correct relative to each magnet's cubic geometry. This could be accomplished with a test setup involving a Helmholtz coil and an integrating flux meter. Samples from two of the manufacturers were confirmed to meet the requirements, with the majority of the samples exhibiting orientation vectors within one degree of the required angle and no vector exceeding an error of three degrees.

2.3 Assembly of magnets and support structure

To qualify the magnet assembly and mounting concept, and to gain insight in preparation for the construction of the full magnet array, our industry partners constructed a tabletop prototype array. The prototype consisted of four magnet drawers, selected from the inboard portion of the full array, mounted in a 2x2 plated structure following the concept used for the full support structure. Various stages of the prototype assembly are photographed in Fig. 2.10.

The construction of the prototype offered an opportunity to practice and improve on a variety of procedures necessary for the construction of the full array. These included the exchange of specification data among project team members to define the required magnet types, locations, and orientations, the production of engineering drawings, gluing the magnets together into blocks, potting the blocks in drawers, assembling the frame for the drawers, and inserting the drawers into the frame against magnetic forces. One especially important insight gained through this process was a critical improvement to the welding procedure for assembling the frame to avoid warping.

2.4 Measurement of magnetic field and verification of its accuracy

The final project objective of PM4Stell was to verify that the magnetic field produced by the assembled magnet array matched the specification to within sufficient accuracy. To meet this objective, it was necessary to develop new test setups and methodology to perform measurements and assess the results. While the project was cancelled before any such measurements could be performed, we describe in this section the preparatory work performed to design a measurement apparatus.

The key measurements to be made in this procedure were the magnetic field vector in the vicinity of the magnet array; specifically, within the volume of space expected to be occupied by the target plasma. Of particular importance is to take measurements on on the boundary of the target plasma equilibrium, as the field on the target plasma boundary was the key criterion used to inform the magnet optimization and verification with the finite-element model.

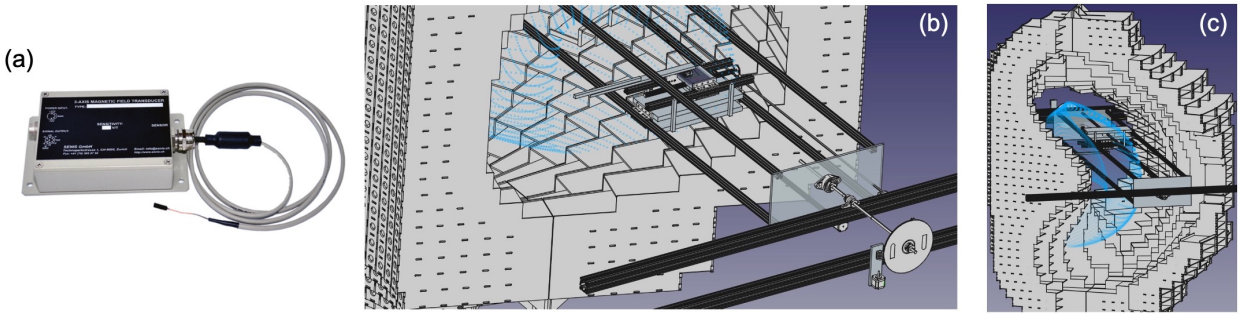

Figure 2.11: Images of the magnetic field measurement apparatus: (a) high-sensitivity Hall probe; (b) close-up view of the moveable stage for the Hall probe; (c) view of the moveable stage positioned within the bore of the magnet array.

These measurements would be performed with a high-sensitivity Hall probe with the capability to measure simultaneously all three components of the magnetic field vector (Fig. 2.11a). A candidate probe has been identified that provides 0.1% measurement accuracy within a background field of 0.2 T and angular orthogonality error of less than 0.1° [12].

The sensor would be mounted on a movable stage with the flexibility to traverse the volume of the bore through the magnet array, such that the probe tip could be positioned, at a minimum, at any point on the virtual surface representing the boundary of the target plasma (Fig. 2.11b-c). The motion of the stage is driven by three independent stepper motors, positioned outside of the regions with highest magnetic field. A LabView-based control system was foreseen, through which the user could specify points in three-dimensional space at which to take measurements.

At least two series of measurements were forseen with the system. The first would take place after the construction and assembly of the main magnet array. This set of measurements would then be used to determine the field errors from array as built due to misalignments and fabrication offsets. These field errors would then be used to specify the positions and polarizations for error-correcting magnets (Sec. 2.1.4). Following the installation of the error-correcting magnets, a second series of measurements would be performed to confirm that the corrected magnet array produced a field with acceptable accuracy according to the physics criteria.

The status of the design of this measurement system was presented at the FDR for PM4Stell. Further design and procurement activities for this measurement system were curtailed when the project was cancelled.

Chapter 3

Summary of project activities

In this section, we will summarize the key activities of the project that led to the deliverables described in Sec. 2. Rather than attempting to describe all project activities at once in chronological order, we have divided the section into key topics and sub-projects. Within each sub-project, we will indicate the chronology primarily with respect to key reference points in the project time line:

Milestone	Date
Proposal submission	December 2019
Proposal acceptance	April 2020
Kickoff meeting of project team	August 2020
Conceptual Design Review (CDR)	March 26, 2021
Preliminary Design Review (PDR)	September 30, 2021
Final Design Review (FDR)	January 14, 2022

3.1 Magnet geometry and positioning

One of the fundamental questions that the project team needed to address in developing a permanent magnet stellarator was what the magnets would look like, and where they should be placed. Because magnet placement for stellarator confinement is an inherently ill-posed problem [13], there is no single solution dictating how the magnets should be designed. The non-uniqueness of the solution is advantageous in the sense that it gave us the flexibility to tailor the magnet geometry for manufacturing feasibility and lower costs.

Our initial concept for the magnet geometry, depicted in the project proposal, was inspired by the trapezoidal cross-sections of magnets in the cylindrical, Halbach-style arrays [14] used to create dipolar or multipolar fields, e.g. in particle accelarators. In an attempt to generalize this concept to the three-dimensional shaping field necessary for stellarator confinement, we arranged magnets tightly around the vacuum vessel for our target plasma and constrained each magnet to have the geometry of a quadrilaterally-faced hexahedron.

The code MAGPIE was initially developed to automate the design and placement of magnets with this geometry, and output from this code was used to develop the project proposal. Depictions of this concept are shown in Fig. 3.1. A preliminary concept for encasing and mounting such magnets was also developed for the proposal (Fig. 3.1a).

This geometry offered the flexibility for magnets to fill the space around the irregularly-shaped vacuum vessel than would have been possible if, for example, all magnets were constrained to have rectangular cross-sections. In that way, the space closest to the plasma boundary—where magnets can have the most impact on the three-dimensional shaping field—could have a higher filling factor of magnet material. Indeed, as described in Ref. [2], the generalized hexahedral magnets were found to be more space-efficient in the sense

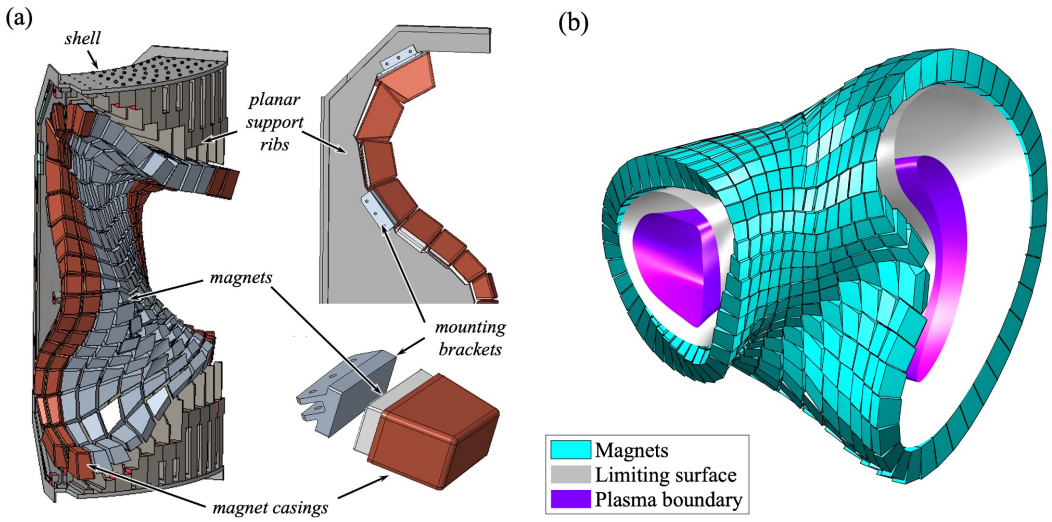

Figure 3.1: Depictions of magnets with hexahedral geometry as presented in the project proposal: (a) preliminary concept for encasing and mounting hexahedral magnets; (b) rendering of hexahedral magnets positioned closely around the vacuum vessel ("limiting surface"). Graphics reproduced from Ref. [2].

that higher field accuracy could be achieved with a lower volume of hexahedral magnets than with magnets with more constraints on their geometry.

A key disadvantage of the hexahedral magnets, however, was the large variation in geometry of each magnet: no two magnets in the arrangement were alike. In addition, initial studies [2] made it clear that constraining the magnets to be polarized along their axes perpendicular to the vacuum vessel—a constraint that would have simplified the fabrication—would preclude the achievement of sufficient field accuracy. Hence, it was decided around the time of proposal acceptance to constrain each magnet to be rectangular to simplify fabrication. Later, approaching the CDR, it was further decided to require every magnet to be a cube with identical dimensions.

The concept for the cubic magnet layout, which essentially remained in effect through the design process, was to group blocks of cubes into wedge-like toroidal sectors (see, for example, Fig. 2.3). In contrast to the arrangements of hexahedra, which formed a grid in the toroidal and poloidal angles around the plasma vessel, the positioning and orientation of the cubic magnet blocks was independent of the shape of the plasma vessel except in the sense that magnets were not placed in areas that would collide with the vessel.

The mounting structure, which will be described in more detail in Sec. 3.4, was designed to enclose magnets arranged according to this concept. As the structural design evolved, the layout of the magnets was tweaked to accommodate features in the structure and to ensure that it was physically possible to mount the magnets. These modifications were implemented as optional features in the MAGPIE code.

3.2 Dipole moment optimization

The basic approach used to determine the magnet parameters necessary to produce the correct magnetic field shaping follows a strategy that has long been used for stellarator coil design. In this approach, the magnet parameters are iteratively adjusted until the normal component of the magnetic field produced by the magnets on the target plasma boundary, including contributions from plasma currents, is zero. Electromagnetic

theory dictates that if this condition is met on the plasma boundary, than the field is correct throughout the plasma volume [15].

The iterative procedure is typically formulated as an optimization problem seeking to limit an objective function F_B related to the square integral of the normal component of the magnetic field on the plasma boundary:

$$F_B = \iint_{\mathscr{S}} \mathbf{B} \cdot \hat{\mathbf{n}} \, dA \tag{3.1}$$

Here, $\mathbf{B}$ is the total magnetic field including contributions from external magnets and plasma currents, $\mathscr{S}$ represents the boundary surface of the target plasma, and $\hat{\mathbf{n}}$ is the unit vector normal to the surface. Commonly the optimizer minimizes not just F_B but rather a weighted sum of F_B and other objective functions representing properties relating to magnet complexity.

A major source of inspiration for our proposal was the insight that this aproach could be used just as well for permanent magnets as for electromagnetc coils [16]. Some early approaches developed for optimizing distributions of permanent magnet material derived from the REGCOIL approach to coil design [17, 18]. However, these approaches used a Fourier parametrization for the permanent magnet geometry, resulting in irregularly-shaped magnetized volumes that would not have been feasible to fabricate.

To move toward more realistic designs, we adopted for this project an approach based on topology optimization. In this approach, the optimizer is provided with a discrete array of magnet dipoles with arbitrary locations. The optimizer then iteratively adjusts their dipole moments to minimize a composite objective function including F_B for a given targe plasma. The advantage of this approach is that it allows the user substantial freedom to specify the layout and geometry of each magnet to accommodate the discrete and irregular features typical of experimental components and mounting structures in a way that would not be feasible if the magnet array had a Fourier parametrization. This approach was implemented in the FAMUS code [3], which was developed for this project as a variant of the existing FOCUS code [4] for coil design.

FAMUS utilizes a quasi-Newton optimization algorithm with the possibility to impose inequality constraints on the optimization parameters. To perform an optimization, the user conceives of an arrangement of magnets, each of which is approximated as an ideal magnetic dipole for the purpose of the optimization. The magnet arrangments for this project were generated by the MAGPIE code to be compatible with the fabrication and mounting concepts described in Sec. 3.4. The input parameters for the optimization include the locations of each magnet in the arrangement, an initial guess for their respective dipole moment vectors, and a maximum allowable magnitude $m_{\max}$. $m_{\max}$ is typically chosen to correspond to the dipole moment of a rare-Earth magnet of the volume allocated for the respective magnet in the arrangement. The optimizer then iteratively adjusts the dipole moments to minimize the total objective function, constraining the moment magnitudes to not exceed $m_{\max}$. Additional inputs for the optimization include fixed parameters including the contribution of plasma currents to the magnetic field, and the magnetic field arising from any electromagnetic coils (which are necessary at least for the purpose of generating a toroidal magnetic field).

If the optimization objective consists solely of F_B, the solution may produce a highly accurate magnetic field, but it will likely have the undesirable property of having many magnets with intermediate dipole moment magnitudes m somewhere between 0 and $m_{\max}$. This is disadvantageous because realizing magnets with intermediate dipole moments would require fabricating magnets in a continuum of sizes less than the volume initially foreseen in the design of the magnet arrangement. We therefore experimented with additional objective functions designed to penalize magnets with intermediate dipole moment magnitudes. The objective function that we eventually adopted was

$$F_\rho = \sum_i^N \left(|\rho_i| \left(1 - |\rho_i|\right)\right)^2, \tag{3.2}$$

where i labels each dipole in the arrangement and ρ is the fractional moment magnitude of each dipole relative to its maximum value $m_{\max}$. In practice, we found that we had the most success when performing the optimization in two stages: first minimizing F_B only, then minimizing a weighted sum $F_B + \lambda F_\rho$, with λ chosen such that in the second stage, the field error metric F_B would remain low while still allowing F_ρ to make a sufficient contribution for magnets with intermediate ρ to be largely eliminated.

This strategy was effective producing highly accurate solutions with binary distributions of relative moment magnitude ρ, such that every magnet in the input arrangement could either retain its full volume for the solution or be removed from the final array altogether. However, these solutions were still impractical. Since the dipole moment directions were treated as continuous optimization variables, every magnet in the solution ended up having a unique polarization orientation. This would have made fabrication prohibitively complex and expensive. Ultimately, it was necessary for the solution to fit within a discrete space with a limited number of possible unique magnet types.

Achieving a discretized solution with high accuracy proved to be challenging. One early approach we tried was to use a generalized version of the F_ρ objective function (Eq. 3.2) that not only penalized intermediate values of the relative moment magnitude ρ but also penalized dipole moment directions that didn't match one of a set of user-supplied permissible directions. However, optimizations with this objective tended to become trapped in local minima of the objective function before reaching solutions with sufficient field accuracy.

Another approach we tried was to abandon the continuous quasi-Newton optimization method altogether and instead optimize the dipole moments with a genetic algorithm. Genetic algorithms have the advantage of being able to perform optimizations within discrete solutions spaces. However, we were unable to find solutions with sufficient field accuracy using this approach. A major challenge of this approach arose from the size of the solution space, which included multiple possible dipole moments for an arrangement of tens of thousands of individual magnets. For such a large solution space, the genetic algorithm required large amounts of memory and computation time, making it difficult to experiment and improve the implementation.

In the end, we were able to find discrete solutions with sufficient accuracy by adding one step to the continuous, quasi-Newton approach. Specifically, after finding a solution with a binary distribution of moment magnitude ρ through the two-stage process described previously, we would simply "round" the dipole moment to the nearest of a prescribed set of allowable polarization vectors. While this rounding procedure would move the solution away from the minimized value of the objective function obtained through the quasi-Newton procedure, sufficient field accuracy could be maintained as long as a sufficient number of allowable discrete vectors were provided. The choice of allowable discrete vectors is described in more detail in Sec. 3.3.

The two-stage continuous optimization followed by the rounding of each dipole moment to the nearest allowable discrete vector, as summarized in Sec. 2.1.3, is described in more detail in Ref. [5].

3.3 Choice of magnet polarization types

The final aspect of magnet design that the project needed to address was to set constraints on the polarization types for each magnet in the array. As discussed in Sec. 3.2, putting no constraints on the polarization of each magnet would likely require each magnet in the array to be unique, thereby complicating the fabrication process. Therefore, it was clear that the polarizations would need to be restricted. On the other hand, too many restrictions on magnet polarization would preclude the attainment of adequate field accuracy. Therefore, the specification of polarization types for the magnets was given extensive consideration.

In the development of the PM4Stell project proposal, it was posited that each magnet could be restricted to be polarized along a single axis defined for each point in the array. This hypothesis arised from the

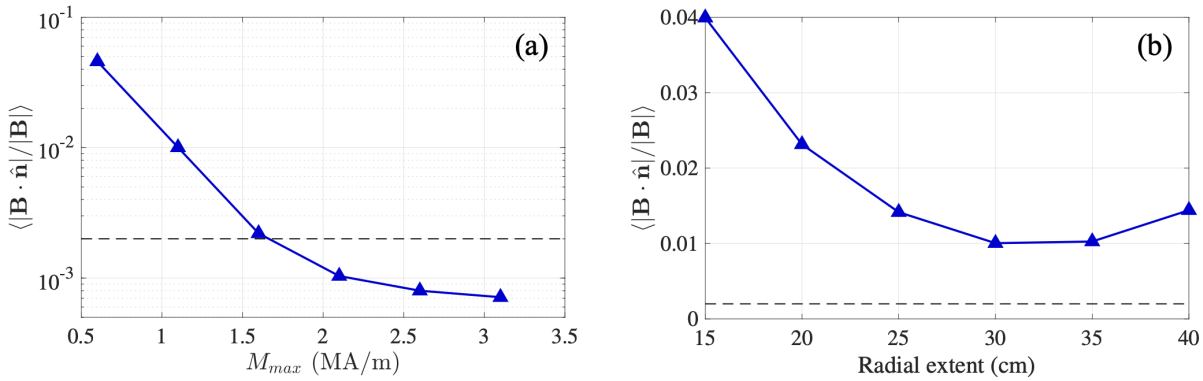

Figure 3.2: Magnetic field error (average relative normal field at the target plasma boundary) obtainable with permanent arrays with vessel-perpendicular polarizations over scans of magnet array parameters. (a) Field error for a scan of allowable dipole moment magnitude, set by the maximum magnetization M_{max}, with the dimensions of the magnet array held fixed. (b) Field error for a scan of magnet layer thickness (radial extent), with the maximum dipole moment magnitude fixed at the rare-Earth permanent magnet level ($M_{max} = 1.1$ MA/m). The horizontal dashed line represents our criterion for maximum allowable field error. Figures reproduced from [2].

observation that, at least in principle, permanent magnets could provide adequate field shaping even if they were constrained to be polarized along axes that were locally perpendicular to a winding surface around the plasma, i.e. the vacuum vessel [17]. In fact, the geometric concept of quadrilaterally-faced hexahedra for the magnets discussed in Sec. 3.1 was developed with this polarization scheme in mind: each of the hexahedral magnets was geometrically oriented along a characteristic axis perpendicular to the vacuum vessel, along which the magnet was foreseen to be polarized.

While such a restriction would simplify the optimization process and magnet fabrication by permitting fewer degrees of freedom, it was found to preclude the attainment of sufficient field accuracy for the target plasma of PM4Stell. As discussed in more detail in [2], when the magnets in the were given this restriction on their polarizations, it was not possible to find a solution with a level of field error below our defined tolerance.

The limiting factor was not the polarization restriction in and of itself, but rather than combination of the restriction on polarization direction and the restriction on dipole moment magnitude according to the strength of available rare-Earth magnets. If we allowed the magnets to have, for example, double the strength of rare-Earth magnets, sufficient field accuracy was obtainable with vessel-perpendicular polarization, as shown in Fig. 3.2a. However, with dipole moment magnitudes consistent with rare-Earth magnets, sufficient field accuracy could only be obtained if the magnets were allowed to have arbitrary polarization directions.

We will note that we also investigated the possibility of using a thicker magnet array while keeping the perpendicular polarization constraint; however, this was also unsuccessful. The results of this investigation are shown in Fig. 3.2b. While thickening the array did offer a marginal improvement in field accuracy at first, further increases to the thickness offered diminishing returns and never reached our criterion. This is likely due to the fact that adding permanent magnets further and further from the plasma has less and less impact on the field shaping at the location of the plasma.

While the constraint of perpendicularly-polarized magnets was shown to be too restrictive for PM4Stell, it has been used successfully in the design of the MUSE stellarator at PPPL [19]. A key difference in the case of MUSE is the lower magnetic field strength requirement. With a lower magnitude of the shaping

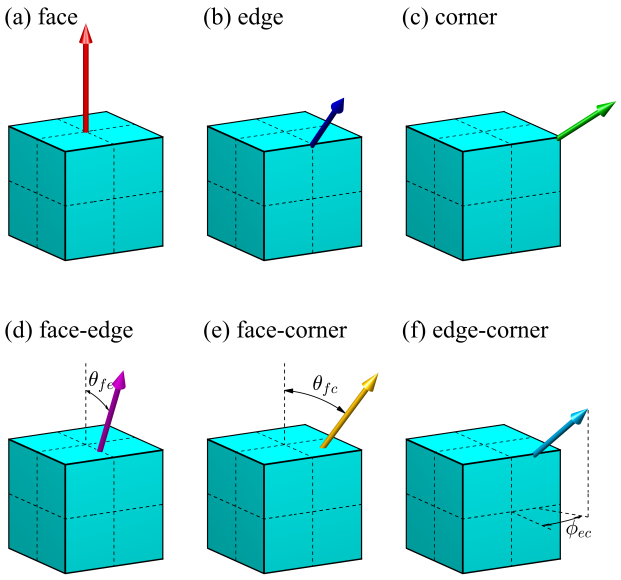

Figure 3.3: Depictions of the polarization types for cubic magnets considered for the design of the PM4Stell magnet array. Reproduced from [5].

field necessary from the permanent magnets, the rare-Earth magnets in the MUSE array are able to produce the required shaping in spite of the relative inefficiency introduced by the perpendicular polarization requirement.

With the possibility of fixing the polarization direction for each magnet thus ruled out for PM4Stell, the task then became determining how many polarization directions would need to be allowed for each magnet. From the point of view of fabrication simplicity, fewer possible polarization directions would be desirable; on the other hand, allowing for more directions increases the likelihood of finding a solution with sufficient field accuracy. We ultimately considered magnets the six polarization orientations shown in Fig. 3.3.

The choice of cubic magnet geometry was helpful for these competing requirements. Taking advantage of the rotational symmetry of the cube's geometry, a single cubic magnet can be used to realize multiple polarization directions within a given place in the magnet arrangement simply by rotating the magnet. For example, a cubic magnet that is polarized perpendicular to a face (Fig. 3.3a) can realize six different dipole moment vectors, i.e. three different axes with two directions along each axis, while maintaining the same geometric footprint. A cube with an oblique polarization can realize more unique dipole moment vectors; for example, if the polarization vector lies in a plane connecting two opposite edges but is not perpendicular to any face (Fig. 3.3e), it can be used to realize 24 distinct dipole moment vectors.

Overall, we considered restricting solutions to six possible subsets of the polarization types shown in Fig. 3.3. The features of these subsets are summarized in Table 3.1. Independently of the magnet arrays or target plasmas to which these subsets are applied, the subsets can be evaluated according to the characteristic quantity θ_{offs}, the maximum angular separation between an arbitrary unit vector and the nearest polarization vector attainable with a subset of polarization types. This can be formally defined on the unit sphere as

$$\theta_{\text{offs}}(\phi,\theta) = \min_{\hat{\mathbf{v}}_s \in S} \left[\arccos\left(\hat{\mathbf{v}}(\phi,\theta)\cdot\hat{\mathbf{v}}_s\right)\right], \tag{3.3}$$

where $\hat{\mathbf{v}}(\phi,\theta)$ is the unit vector with azimuthal angle ϕ and polar angle θ, s labels a polarization direction within subset S, and $\hat{\mathbf{v}}_s$ is the unit vector associated with polarization direction s. Distributions of θ_{offs} for some example subsets are shown in Fig. 3.4.

Two helpful metrics to characterize each subset were the maximum attainable value, as well as $\|\theta_{\text{offs}}\|_2$, the square root of the integral of θ^2_{offs} over the unit sphere. These metrics are both included in Table 3.1

Subset	F	E	C	FE	FC	EC	θ_{fe}	θ_{fc}	ϕ_{ec}	Num. of polarizations	Max. θ_{offs} (deg.)	$\|\theta_{\text{offs}}\|_2$ (deg.)
1	✓									6	54.7	34.0
2	✓	✓								18	35.2	19.9
3	✓	✓	✓							26	27.5	16.6
4	✓	✓		✓			22.5			42	35.2	16.2
5	✓			✓	✓		30.3	38.1		54	19.4	11.3
6		✓		✓	✓		18.4	38.6		60	18.4	10.6
7	✓	✓		✓	✓		22.5	38.6		66	16.9	10.2
8	✓	✓	✓	✓	✓	✓	22.5	27.0	22.5	98	14.1	8.50

Table 3.1: Properties of the subsets of polarization types considered in this work. Check marks indicate the presence of a given type in each set. The types are abbreviated as follows: F=face, E=edge, C=corner, FE=face-edge, FC=face-corner, and EC=edge-corner. Angular parameters for the hybrid types (θ_{fe}, θ_{fc}, ϕ_{ec}), as defined in Fig. 2.1, are given if their respective types are included in the subset.

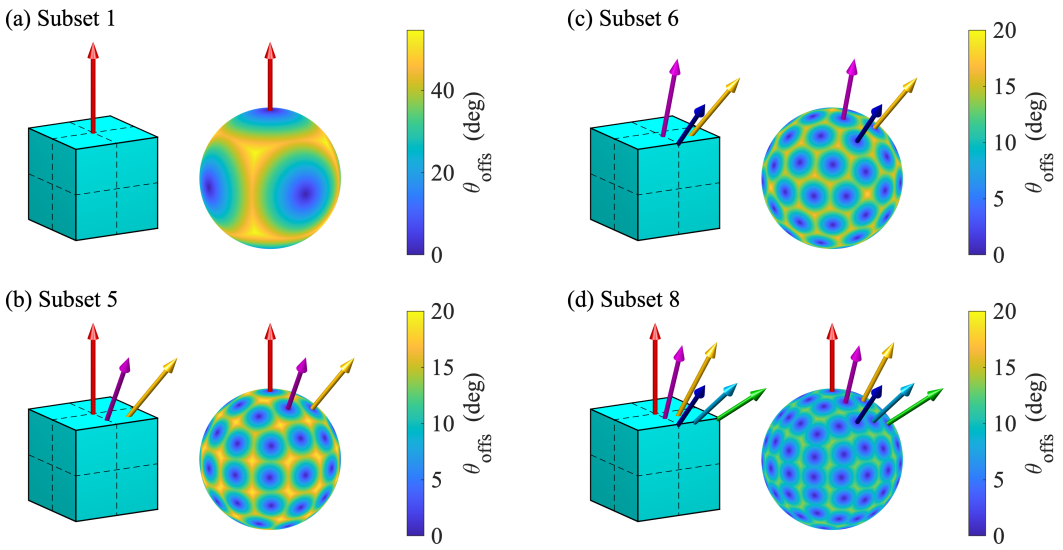

Figure 3.4: Example polarization vectors relative to a cubic magnet (left side of each subfigure) and distribution of θ_{offs} over the unit sphere (right side) for a selection of the polarization type subsets specified in Table 3.1. Note that the color scale for Subset 1 (a) is different from that of the others (b)-(d). Figure reproduced from [5].

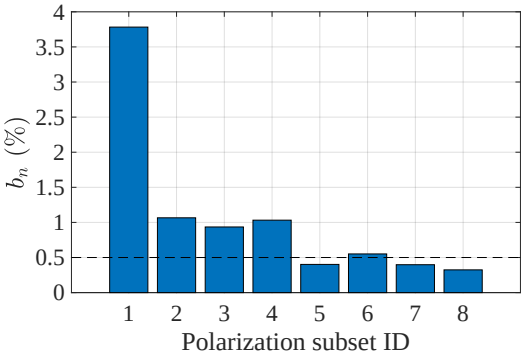

Figure 3.5: Mean normalized error field on the boundary of the target plasma obtained with solutions using the eight polarization subsets described in Sec. 3.3. The horizontal dashed line indicates the threshold criterion for acceptable field error. Figure reproduced from [5].

for each subset considered in this work. In general, both quantities tend to decrease with the number of allowable polarization vectors. In some cases, the characteristic angles between allowable vectors in a given subset were fine-tuned to minimize $\|\theta_{\text{offs}}\|_2$.

To evaluate the suitability of each subset for the PM4Stell target plasma, we computed the field accuracy of a magnet array defined by rounding each magnet from the solution with continuous polarizations—determined in step 2 of the procedure summarized in Sec. 2.1.3—to the nearest allowable dipole moment as permitted by the respective subset, as described in step 3 of the procedure. The mean normalized field error obtained for each subset is shown in Fig. 3.5.

Note that, as shown in Fig. 3.5, field error tends to trend downward with $\|\theta_{\text{offs}}\|_2$ (Table 3.1), but not monotonically. Furthermore, the solution using Subset 5 attains nearly the same field accuracy as Subset 8, despite including only half as many types of magnets. Because of this, we chose the polarization types within Subset 5 for the PM4Stell solution, thereby limiting the number of unique magnets to three. The sufficiency of the solution using Subset 5 was further verified through VMEC free-boundary modeling, indicating that the plasma attainable with this solution was very close to the target plasma (Fig. 2.6).

3.4 Mounting structure

The design of a structure to hold the permanent magnets in place proved to be especially challenging, as the structure needed not only to withstand the weight of the magnets, but also the substantial electromagnetic forces that the magnets exerted on one another. Moreover, the design needed to facilitate a viable procedure for assembling the magnet within the structure in the face of substantial electromagnetic forces that could change dramatically as the magnets were moved into place.

The earliest concept for magnet mounting was developed in the process of writing the proposal. Shown in Fig. 3.1, it was developed largely to accommodate the hexahedral magnet arrays that were foreseen at that time, described in Sec. 3.1. Each hexahedral magnet would be enclosed in a case, which would in turn be fastened to a vertical sheet-like "rib" structure. Each rib would lie in a plane of constant toroidal angle. As the hexahedral magnet concept was abandoned in favor of simpler geometric concepts shortly after the acceptance of the proposal, the associated mounting concept was not studied in detail for structural soundness or feasibility of mounting.

By the time of the project kickoff, magnet geometries had been restricted to be rectangular prisms, and later cubes (Fig. 2.3). In these concepts, the magnets were positioned in wedge-like toroidal sectors, narrow at low major radii and wide at higher major radii. Unlike the hexahedral magnet concept, the magnet shapes were independent of the shape of the plasma boundary or vacuum vessel. Within each wedge, the magnets were positioned in a regular grid in the major radial (r) and vertical (z) dimensions.

Two structural concepts were explored to accommodate these types of magnet arrangements. In the first, referred to as the *honeycomb*, each wedge of magnets would be stored in a designated structure, as shown in

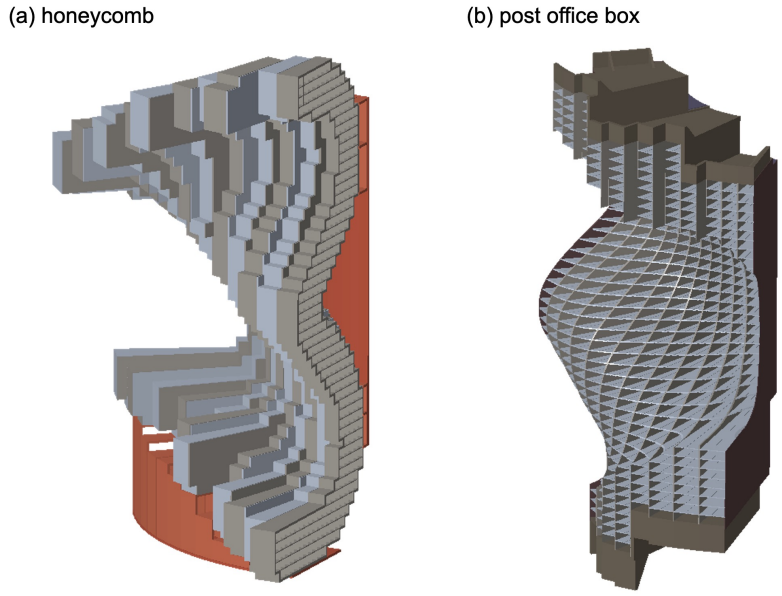

Figure 3.6: Renderings of the inboard-side components of early iterations of two magnet mounting concepts: (a) honeycomb; (b) post office box.

Fig. 3.6a. The magnets would be installed from the side and inserted in the toroidal dimension. To assemble the magnet array in this concept, wedges would need to be placed and loaded one-by-one, as the magnets within a wedge would be inaccessible once the neighboring wedge was put into place.

The second concept, referred to as the *post office box*, was more interconnected in the toroidal dimension. Rather than consisting of many tall structures enclosing individual wedges, the post office box consisted of a grid of interlocking plates in the toroidal and vertical dimensions, as shown in Fig. 3.6b. In contrast to the honeycomb concept, magnets in the post office box concept would be inserted in along the major radial dimension.

After some early development of both concepts, the post office box quickly appeared to be the more robust option. The tall, thin structures constituting the honeycomb array would be subject to warping under the magnetic forces, making it difficult to achieve adequate misalignment tolerances. The requirement for insertion along the toroidal dimension would be challenging and would lead to risks of ejecting magnets during the assembly process. In addition, large forces were expected when installing subsequent wedges into the array. On the other hand, the post office box concept offered advantages in these areas. The post office box structure enabled the subdivision of magnets into drawers with steel casings (Fig. 2.2b) that could be more easily controlled during the insertion process. Furthermore, the gridded plate structure was more robust against warping and misalignment and involved fewer large assemblies to handle. Therefore, by the time of the CDR, the post office box concept was adopted for more detailed design efforts.

In the final design, the support structure was divided into four main components, shown in Fig. 3.7. Each component consists of interlocking steel plates, welded together to form a cylindrical grid of "post office box"-like cubbies into which drawers of magnets can be inserted in the radial direction. The structure for the inboard side of the stellarator half-period is a single, unified component (Fig. 3.7a), whereas the structure for the outboard side of the half-period is divided into three components (Fig. 3.7b).

The plates in each structure are foreseen to be manufactured by waterjet cutting. Originally, the plates had grooves to guide the insertion of magnet drawers. However, after considering the tooling system that our industrial partners planned to use to insert the drawers, it was determined that the grooves were not necessary and therefore removed from the design. This saved cost by eliminating the need for any machining of the plates, a process that would have been unwieldy given the plates' sizes and shapes.

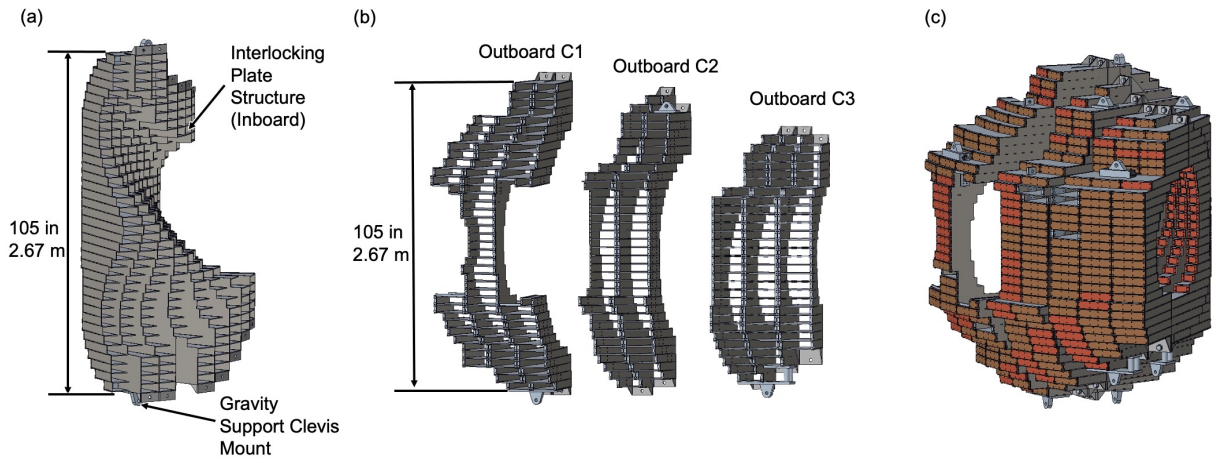

Figure 3.7: CAD renderings of the main structural components used to hold the magnets in the array: (a) inboard structure; (b) outboard structures; (c) all four structural components, assembled and filled with magnets.

3.5 Tolerances and error correction

As the magnets, drawers, and mounting structure were each subject to inaccuracies in fabrication and alignment, it was important to document the tolerances and determine whether they were acceptable. For PM4Stell, the critical factor to qualify the tolerances was the magnetic field accuracy, and in particular whether error fields arising from these inaccuracies within the tolerances could be corrected with the error-correcting magnet array described in Sec. 2.1.4.

The main tolerances for the magnet array are summarized in Table 3.2. The first four error types in the table concern the fabrication of individual magnets and were set empirically according to measurements performed on samples ordered from a vendor (Sec. 2.2). Systematic magnetization and polarization errors are deviations of the dipole moment magnitude and orientation by the same amount for every magnet in the array of a given polarization type. Random magnetization and polarization errors, by contrast, are independent deviations of each individual magnet from its specification. Frame torquing is the twisting of the frame in response to magnetic forces. Drawer misalignment is a spatial offest of all the magnets in a given drawer. Mounting structure misalignment refers to spatial offsets of the four main mounting structures as shown in Fig. 3.7. Finally, glue-up error refers to offsets between magnets due to discrepancies in the thickness of the glue layer.

To design of the error-correcting magnet array, further functionality was added to MAGPIE to place this secondary array of magnets between the main magnet array and the vacuum vessel while maintaining requirements for gap spacing and mountability. To determine the polarizations required for the error-correcting magnets to correct a given set of offsets, we used the same optimization procedure as for the main magnet array (Sec. 3.2). As described in more detail in Sec. 2.1.4, the magnets were shown to be able to adequately correct the field errors that might arise due to offsets within the tolerances.

Error type	Standard deviation	Max. allowable error	Units
Systematic magnetization	3	5	%
Systematic polarization	1	2	degrees
Random magnetization	1.5	3	%
Random polarization	2	3	degrees
Frame torquing	0.025	0.05	degree m^{-1}
Drawer misalignment (radial)	1.5	3	mm
Drawer misalignment (vertical)	0.5	2	mm
Mounting structure misalignment	1	2	mm
Glue-up error	0.075	1.15	mm

Table 3.2: Summary of the tolerances for fabrication and alignment for the PM4Stell magnet array.

3.6 Design workflow automation

The PM4Stell permanent magnet array consists of tens of thousands of individual magnets packaged into hundreds of drawers, almost all of which contain a unique arrangement of magnets and/or a unique size. Given the complexity of the design, it was crucial to develop automated procedures to speed the design process and allow for iterations to improve the design to address flaws and weaknesses. The automation was facilitated through a combination of macro script writing capabilities within the design and analysis software programs, as well as dedicated software and procedures for workflow management.

The PM4Stell project benefitted greatly in this area from a separate PPPL initiative to develop *virtual engineering* capabilities. This initiative, which was supported by indirect funds from the PPPL engineering department, fortuitously chose the PM4Stell project as a test bed for virtual engineering. Through this program, our project team had access to advanced software licenses as well as direct assistance by experts from the Ansys team at no additional cost to the project.

One example of a process that benefitted greatly from automation was the design of the mounting structure described in Sec. 3.4. Consisting of tens to hundreds of plates of varying dimensions, the structure would have taken prohibitively long to design "by hand." To automate the process, we took advantage of the *family tables* feature in the Creo CAD software. This feature provides a compact way to specify a series of similar components from a template component with a set of user-defined parameters for attributes such as dimensions, spatial positions, orientations. We could therefore automate the design process for the structure by writing a script that would read the physics specification files output by the MAGPIE and FAMUS for the magnet positions, determine the required positions, dimensions, and orientations for the plates required to enclose the magnets, and populate the families of tables accordingly.

Another application of automation procedures was the development of a finite element model of the magnet array for the high-fidelity magnetic field calculations described in Sec. 2.1.5. Since the model involved 35,436 individual magnets, it simply would not have been possible to build up model with no automation. As such, we used the Ansys SpaceClaim program to create the finite element model for each magnet, utilizing a custom script that would read in the geometric and dipole moment specifications from the MAGPIE and FAMUS output files. The model would then be loaded into the Ansys Maxwell software for a detailed calculation of the magnetic field.

As highlighted in the above two examples, the workflow involved complex transfers of specification and model data between many different software programs (and different team members) in a many different file formats. This coordination was facilitated by the creation of a detailed specification of file formats for data exchange, as well as the use of the Ansys Minerva workflow automation software program.

3.7 Finite element modeling of magnetic fields and stresses

Before undertaking to construct the magnet array, it was important to build as much confidence as possible in the ability of the array to produce the required magnetic field to the required accuracy as well as to withstand the large forces anticipated between the magnets. To this end, we employed high-fidelity finite element modeling to qualify the design and inform refinements. For calculations of the magnetic field, we used Ansys Maxwell software; for structural forces; we used Ansys Mechanical.

3.7.1 Magnetic field

As briefly described in Sec. 3.6, we build finite element models of the magnet array in the Ansys Maxwell program using an automated procedure. The source material for the models came from two output files from the physics design codes (MAGPIE and FAMUS): a "blocks" file that provided the locations, dimensions, and orientations of each cubic magnet in the array, and a "moments" file that provided the magnetic dipole moment vector assigned to each of the magnets. From these source files, the model was constructed with the help of a custom script and Ansys SpaceClaim.

The large number of individual magnets combined with the stringent requirements for field accuracy proved to be a demanding application for the high-fidelity modeling software. Initially, the computation times for both constructing the model and running the field calculation were prohibitively long (multiple days). Our team was fortunately able to speed up both of these processes considerably. For the model construction, our Ansys partners found some opportunities to streamline parts of the Ansys software base to exploit patterns within our designs to make the process more efficient.

For the magnetic field calculation, one initial roadblock arose from the fact that the magnet design included small gaps between each magnet to account for the presence of glue. The multitude of small gaps within a large magnet array required the generation of an especially large number of small elements, leading to long computations that sometimes failed to converge to a solution. However, since the precise value of the magnetic field within these gaps was unimportant for our purposes, we created a modified model in which the magnets were slightly expanded so as to eliminate the gaps. The intrinsic magnetization of each magnet was correspondingly reduced such that its dipole moment remained the same according to the physics design specification. The elimination of the gaps greatly simplified the mesh generation and made the field calculation more tractable.

As we developed ways to improve and streamline the finite element model itself, we pursued a stepwise approach to performing the magnetic field calculations. The initial step involved similar simplifying assumptions as those used by the physics optimization codes, whereas successive steps added increasingly complex and nonlinear features to the magnets. Specifically, the first step made the simplifying assumption of a unit relative magnetic permeability, such that the calculation was fully linear. Next, we set the relative permeability of the magnets to 1.05, more representative of rare-Earth permanent magnets but also more complex because the permeability was no longer uniform through the simulation volume. We then proceeded further to simulate magnets with nonlinear B-H curves, which most accurately represented the properties of the N48M magnet material that we intended to use for the array. We also defined a coercivity for each magnet, i.e. the field above which the magnet would demagnetize. The resulting instances of demagnetization were summarized in Sec. 2.1.5 (see in particular Fig. 2.8).

Ultimately, we produced two different finite element models for field calculations. The first was meant to calculate the field from the array as we planned to construct it for the PM4Stell project: one half-period's worth of magnets, with no toroidal-field (TF) coils. This was most useful for predicting the forces to be expected on the mounting structure, as well as the field distributions that we could expect to measure in the procedure described in Sec. 2.4. The second model was used to calculate the field that would be produced if we were to construct a complete stellarator according to the half-period design, and included TF coils.

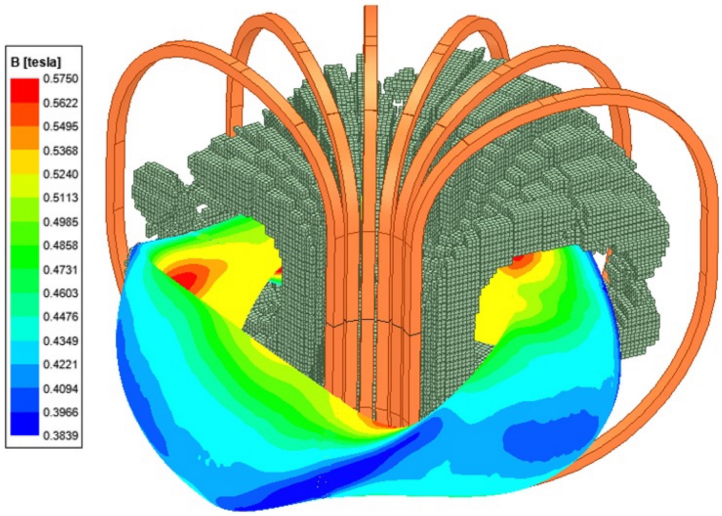

Figure 3.8: Rendering of the magnets and TF coils used in the finite-element calculation of the field produced by the full stellarator that formed the basis for the design. Magnets and coils are shown for one half-period of the stellarator. The strength of the resulting magnetic field on the boundary of the target plasma is also shown.

This was most useful to verify that the design could meet the fundamental requirements for confining a stellarator plasma. It was fortunately not necessary to model every magnet in the stellarator; rather, the model only explicitly contained the magnets within a single field period and applied cylindrical periodic boundary conditions to the toroidal planes on each end of the field period. A rendering of the model and the resulting field calculation is shown in Fig. 3.8.

3.7.2 Structural forces

With the magnetic field thus calculated throughout the spatial volume occupied by the magnet array, it was then possible to determine the stresses expected on the mounting structure. These were determined in a separate finite-element model built in the Ansys Mechanical program. The key inputs were the magnetic field result from Ansys Maxwell and a model of the structure.

For purpose of stress and strain calculations, it was for the most part not necessary for the structural model to include all the fine details of the original design (Sec. 3.4). Rather, to save computational expense, a simplified model was constructed that preserved only the key features expected to be consequential for the distribution of stresses throughout the structure, such as slots and weld seams. Comparisons of the CAD model of the structure with the model used for mechanical analysis are shown in Fig. 3.9. As with the CAD model, construction of the mechanical model was facilitated with automation scripts and Ansys SpaceClaim.

Calculations of forces within the simplified global model helped to identify critical parts of the design that would experience the largest stresses. To study the critical areas more closely, we created detailed breakout models that contained the geometry and composition of parts as specified in the CAD model. The breakout models mostly concerned components that fastened large parts of the structure together, such as the joints shown in Fig. 2.9b-c. The results from the both the global and breakout models helped to inform modifications to the design to make it more resilient to the anticipated loads.

3.8 Magnet array prototype

An important step in qualifying the design of the magnet array and retiring the main risks was the construction of a small prototype magnet array. Consisting of a grid of four “post office boxes” populated with magnet drawers, it enabled us to qualify the array design, assess which aspects of the design needed re-

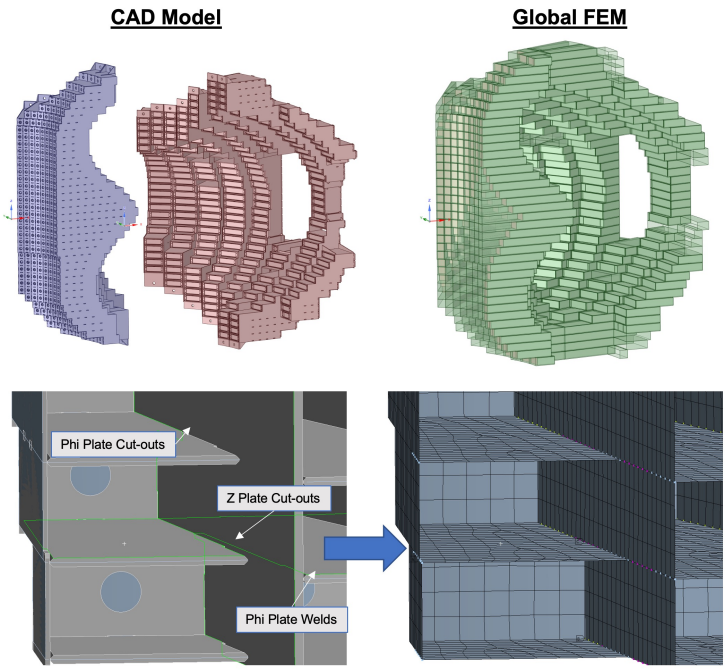

Figure 3.9: Comparison of the CAD model of the support structure (right column) with the model used for mechanical stress calculations (left column). The top row shows an overview of the full structure (divided into inboard and outboard parts for the CAD model); the bottom row shows a detailed view of one section of each model.

finement, and develop tooling and best practices for assembling the drawers of magnets and mounting them within the structure.

The magnet drawers for the prototype were designed to match a set of four drawers within the inboard side of the PM4Stell design. They included combinations of magnets of all three of the polarization types illustrated in Fig. 2.1, as well as cubes of Garolite that occupied positions within the magnet arrangement that required a dipole moment of zero. Fig. 2.10a shows a block magnets and Garolite cubes for one drawer glued together; Fig. 2.10b shows a completed magnet drawer, in which the magnet block is potted in epoxy and enclosed within a stainless steel casing.

A serious issue arose during the first attempt to assemble the mounting structure for the prototype. The interlocking plates became warped after they were welded together, to the extent that the magnet drawers could not be installed. After investigating the issue, it was determined that the main cause was the accumulation of heat in the plates during welding, resulting in uneven thermal expansion. The procedure was therefore modified in several ways, including the incorporation of fixtures that would help to remove heat from the structure as well as simply allowing more time for the structure to cool down after each weld. With these new procedures in place, PPPL engineers constructed a welded mockup box to demonstrate that they were sufficient to avoid the warping.

3.9 Proposals for scaled-down magnet arrays

Between the submission of the initial project proposal and the completion of the final design review, the price of rare-Earth permanent magnet material increased more than threefold. Since this material was a major driver of the project cost, it was clear that the PM4Stell magnet array could not be built within the constraints of the original project budget.

Following the FDR, the team brainstormed some options for constructing an array with fewer magnets to reduce the overall cost. One candidate descoped array is illustrated in Fig. 3.10. While the resulting magnetic field would not be the same as that which would have been produced by the full half-period array

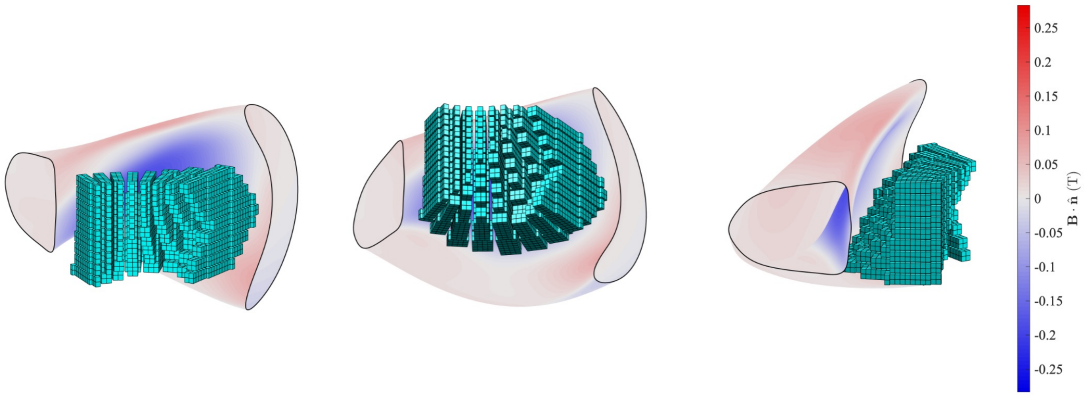

Figure 3.10: Renderings of the magnets within a descoped version of the PM4Stell array along with the normal component of the magnetic field that they would generate on the boundary of the target plasma equilibrium.

as originally proposed, it would still create a nontrivial spatial distribution. Therefore, the descoped array could still be used to qualify the field measurement and error correction procedures and thereby provide a useful validation of the methodology developed in this project. In addition, the descoped array would still entail the construction of the full inboard-side mounting structure, thereby offering a validation of the construction procedure. The descoped magnet array was also much larger than the four-drawer prototype, and would therefore expand our team's experience in assembling such arrays.

However, even with the reduced magnet quantities, the total project cost would still exceed the original budget by about $1.12 M. This remaining overshoot was driven in larger part by higher-than-expected expenses for the tooling used for magnet assembly.

Chapter 4

Products and technology transfer activities

4.1 Peer-reviewed journal publications

1. C. Zhu, K. C. Hammond, M. Zarnstorff, T. Brown, D. Gates, K. Corrigan, M. Sibilia, and E. Feibush, "Topology optimization of permanent magnets for stellarators", *Nuclear Fusion* **60**, 106002 (2020)

2. K. C. Hammond, C. Zhu, T. Brown, K. Corrigan, D. A. Gates, and M. Sibilia, "Geometric concepts for stellarator permanent magnet arrays", *Nuclear Fusion* **60**, 106010 (2020)

3. C. Zhu, K. C. Hammond, A. Rutkowski, K. Corrigan, D. Bishop, A. Brooks, P. Dugan, R. Ellis, L. Perkins, Y. Zhai, A. Chambliss, D. A. Gates, D. Steward, C. Miller, B. Lown, and R. Mercurio, "PM4STELL: a prototype permanent magnet stellarator structure", *Physics of Plasmas* **29**, 112501 (2022)

4. K. C. Hammond, C. Zhu, K. Corrigan, D. A. Gates, R. Lown, R. Mercurio, T. M. Qian, and M. C. Zarnstorff, "Design of an arrangement of cubic magnets for a quasi-axisymmetric stellarator experiment", *Nuclear Fusion* **62**, 126065 (2022)

5. A. Rutkowski, K. Hammond, C. Zhu, D. A. Gates, and A. Chambliss, "A novel scheme for error field correction in permanent magnet stellarators", *Nuclear Fusion* **63**, 026027 (2023)

4.2 Conference presentations

Oral presentations:

1. K. C. Hammond, "Geometric concepts for stellarator permanent magnet arrays," 62nd Annual Meeting of the APS Division of Plasma Physics, hosted virtually, November 9-13, 2021.

2. C. Zhu, "Stellarators with permanent magnets," 2021 Max Planck Princeton Center Annual Meeting, hosted virtually, January 19-22, 2021.

3. A. Chambliss, "Application of the shape gradient and Hessian matrix methods to compute the sensitivities of magnetic islands in permanent magnet stellarators," Sherwood Fusion Theory Conference, August 16-18, 2021.

4. C. Zhu, "Stellarator simplification using permanent magnets," **invited talk**, 63rd Annual Meeting of the APS Division of Plasma Physics, Pittsburgh, PA, USA, November 8-12, 2021.

5. D. Gates, "Stellarator simplification using permanent magnets," 30th International Toki Conference, November 18, 2021.

6. K. Corrigan, "Structural concepts for stellarator permanent magnet arrays," 29th IEEE Symposium on Fusion Engineering, December 12-16, 2021.

7. K. C. Hammond, "Design and optimization of a quasi-axisymmetric stellarator with permanent magnets," **invited talk**, 23rd International Stellarator-Heliotron Workshop, Warsaw, Poland, June 20-24, 2022.

Posters:

1. M. C. Zarnstorff, "Opportunities for reduced cost stellarator pilot plants," 62nd Annual Meeting of the APS Division of Plasma Physics, hosted virtually, November 9-13, 2020.

2. C. Zhu, "Design of a permanent magnet stellarator," 62nd Annual Meeting of the APS Division of Plasma Physics, hosted virtually, November 9-13, 2020.

3. D. A. Gates, "Stellarator simplification with permanent magnets," 28th IAEA Fusion Energy Conference, hosted virtually, May 10-15, 2021.

4. C. Zhu, "Towards simpler coils for optimized stellarators," 28th IAEA Fusion Energy Conference, hosted virtually, May 10-15, 2021.

5. K. C. Hammond, "Design of an arrangement of cubic magnets with discrete polarizations for a quasi-axisymmetric stellarator experiment," 62nd Annual Meeting of the APS Division of Plasma Physics, Pittsburgh, PA, USA, November 8-12, 2021.

4.3 Patent applications and licensing agreements

1. K. C. Hammond, C. Zhu, and D. A. Gates, "Stellarators using arrays of permanent magnets," Provisional U.S. Patent No. 63/319,568, filed March 14, 2022.

2. D. A. Gates, C. Zhu, and K. C. Hammond, "Planar coil stellarator," Provisional U.S. Patent No. 63/319,580, filed March 14, 2022.

The inventions listed above are subject to an exclusive license between the Trustees of Princeton University and Princeton Stellarators, Inc.

Chapter 5

Work involving computer modeling

The objective of the PM4Stell project entailed the design of a complex array of tens of thousands of magnets with the requirement to create a magnetic field with precise shaping requirements. To make this design effort possible, we relied heavily on computer codes to model the magnetic field produced by the magnets. The codes were integral for multiple aspects of the design, including specifying the required polarization orientations, qualifying the array for field accuracy in the presence of non-ideal magnet effects, and determining the fields and resulting forces between the magnets. In this chapter, we summarize the main software programs used for this modeling, as well as our efforts to validate the results.

5.1 Optimization with FAMUS and the dipole approximation

As described in Sec. 3.2, the FAMUS code was used for the fundamental design task of determining the required polarizations for each magnet in the PM4Stell array. Output from FAMUS has been presented in a number of peer-reviewed publications, including work for PM4Stell [1–3, 5, 6] and other projects [18–20]. The source code and documentation may be accessed at https://github.com/PrincetonUniversity/FOCUS under the "dipole" branch.

FAMUS uses an optimization procedure to iteratively adjust the dipole moments of each magnet in order to minimize the deviation of their collective magnetic field at a set of test points located on the boundary of the target plasma equilibrium. Performing this optimization requires hundreds of field evaluations, each of which entails calcuating the field created by tens of thousands of magnets at thousands of test points. In addition, the quasi-Newton approach employed in FAMUS requires information on the derivatives of the field at the test points with respect to changes in the magnets' properties.

Given the number of such calculations required, it is necessary to make simplifying assumptions about the magnets for the optimization procedure to be feasible. Specifically, FAMUS treats each magnet as an idealized point dipole located at the magnet's center of mass. With this approximation in place, the field at any test point can be calculated simply as the sum of contributions from each point dipole in the array, given by the well-known formula from electromagnetics:

$$\mathbf{B} = \frac{\mu_0}{4\pi} \sum_i \left(3 \frac{\mathbf{m}_i \cdot \mathbf{r}_i}{|\mathbf{r}_i|^5} - \frac{1}{|\mathbf{r}_i|^3} \mathbf{m}_i \right), \tag{5.1}$$

where μ_0 is the vacuum permeability constant, the index i labels each magnet in the array, $\mathbf{m}_i$ is the dipole moment of the ith magnet, calculated as the product of the magnet's volume times the intrinsic magnetization of rare-Earth magnets, and $\mathbf{r}_i$ is the vector from the magnet's center of mass to the test point.

This approximation neglects the finite dimensions of the magnet and therefore will exhibit errors in the area near and inside the boundary of the magnet, most severely near the center of mass where the field

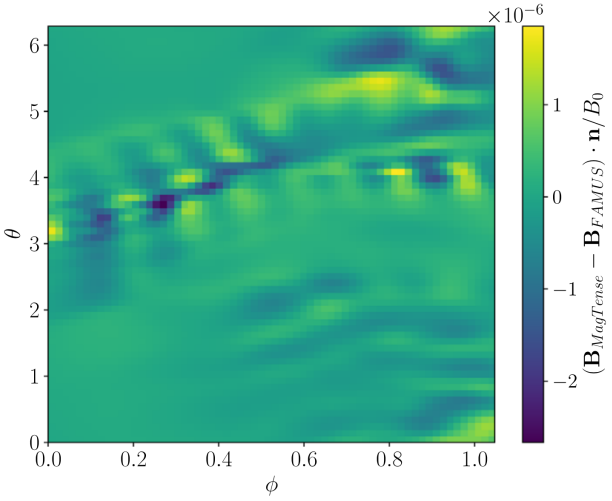

Figure 5.1: Difference in the normal component of magnetic field the magnet array, calculated using the dipole approximation (B_{FAMUS}) and the with magnets of finite dimensions and uniform magnetization ($B_{MagTense}$) from one on the boundary of the target plasma and normalized to the field on axis (0.5 T). The plasma boundary is parametrized according to toroidal angle ϕ and poloidal angle θ. Reproduced from [1].

strength approaches infinity. In addition, the approximation neglects the effects of the the permeability of the permanent magnets, which in general is different from that of free space and therefore affects the shaping of the magnetic field. In addition, the approximation neglects the coercivity of the magnets, which would cause them to demagnetize if the ambient field exceeds a certain level in the direction antiparallel to the magnet's polarization.

Due to these approximations, the optimization algorithm effectively optimizes the dipole moments to generate a field that differs from the one that is actually required for the target plasma. To ensure that our design met the requirements for field accuracy, therefore, it was important to quantify the discrepancy between the field predicted by the optimizer and the field actually produced by the array of permanent magnets when constructed according to the specification provided by the optimizer.

To evaluate the effect of neglecting the finite spatial dimensions of the magnets, we compared the magnetic field calculations performed by FAMUS to those performed by MAGTENSE, the latter of which used an analytic formula to evaluate the field from magnets with rectangular geometry.[10, 11]. The relative discrepancy in the field at test points along the target plasma boundary, as shown in Fig. 5.1, was found to be negligible. This is likely because the plasma boundary lies in the "far-field" region for all of the magnets in the array, i.e. it is far from each magnet relative to the individual magnet dimensions. Hence, this particular error source contributes negligibly to offsets in the FAMUS optimization.

It should be noted that, in contrast to the plasma boundary, the mounting structures do not lie in the far-field region. Hence, the dipole approximation is not suitable for determining forces within the structure. However, as long as these forces are not considered in the magnet optimization, the dipole approximation may be used for optimization purposes. On the other hand, when calculating these forces to assess the suitability of the structure (Sec. 3.7.2), we used a higher-fidelity field calculation.

More substantial errors arise from neglecting the material properties of the magnets; in particular, their permeability. To calculate offsets to the FAMUS calculation arising from the permeability of the magnets, we performed another calculation with MAGTENSE, this time with the relative permeability $\mu_r = 1.05$, comparable with that of rare-Earth permanent magnets. As shown in Fig. 5.2a, the model with $\mu_r \neq 1$ produces a substantially larger discrepancy relative to the dipole approximation than the model with finite volume but $\mu_r = 1$ (Fig. 5.1). However, these discrepancies are well within the range that is correctable by the error-correcting magnets. As shown in Fig. 5.2b, after optimizing the error-correcting magnet array to correct the discrepancies shown in Fig. 5.2a, the discrepancies have nearly vanished.

For an even higher fidelity calculation of the magnetic field, which does not assume a linear permeability but rather takes full account of the nonlinear B-H curve of the permanent magnets, we developed a finite-

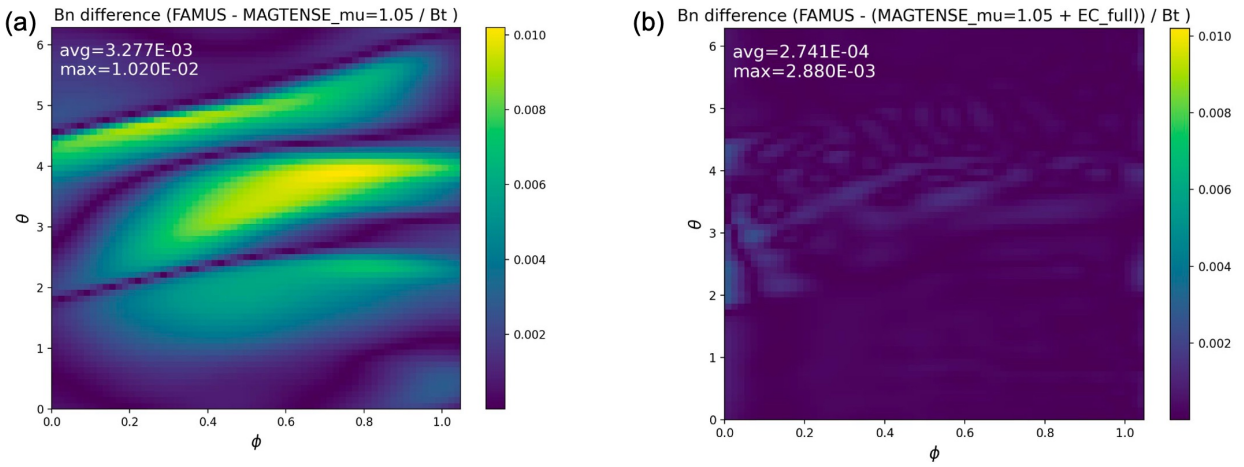

Figure 5.2: Comparisons between calculations of the magnetic field at test points on the plasma boundary using the dipole approximation (with FAMUS) and with finite-volume magnets with relative permeability $\mu_r = 1$ (with MAGTENSE). (a) Difference between the two calculation methods relative to $B_t = 0.5$ T; (b) Difference after adding contributions from error-correcting magnets that have been optimize to cancel out the discrepancy.

element model in Ansys Maxwell as described in Sec. 2.1.5 and 3.7.1. As shown in Fig. 2.7 the offsets in magnetic field calculated at the target plasma boundary are comparable in magnitude to those of the calculation assuming linear permeability (Fig. 5.2b) and therefore can be similarly be corrected with the error-correcting magnets.

5.2 Finite element modeling with Ansys Maxwell

Ansys Maxwell [21] is a widely-used commercial finite-element code for simulating static and low-frequency electomagnetic fields. Its key capabilities for the purposes of this project included automatic, adaptive meshing and simulation of permanent magnets with nonlinear B-H curves. As described in Sec. 2.1.5 and 3.7, the software was instrumental in verifying the accuracy of the magnet design and evaluating the magnetic field within the magnet array for the structural force calculations. However, attaining the fields to sufficiently high fidelity required the development of a complicated and computationally demanding model, and in the course of its development the project team performed a number of consistency checks to verify that the model was working as intended.

A first step was to confirm that the field calculation on the target plasma boundary performed by Ansys Maxwell with the assumption of $\mu_r = 1$ reasonably matched that of FAMUS. While the results are not expected to be exactly the same due to the finite size of the magnets in the Ansys Maxwell model, as shown in Sec. 5.1, this effect creates a negligible discrepancy at locations on the plasma boundary.

A comparison of the FAMUS calculation and the ANSYS calculation with $\mu_r = 1$ is shown in Fig. 5.3a for the fields on one field period of the plasma boundary, taking contributions from the magnets and TF coils for a full stellarator. Ideally, this result should be of a similar magnitude to the FAMUS-MAGTENSE comparison with $\mu_r = 1$ shown in Fig. 5.1; however, substantially larger discrepancies are observed. However, these discrepancies are largely random in nature and exhibit little to no noticeable large-scale spatial structure (for comparison, see the FAMUS-MAGTENSE discrepancy with $\mu_r = 1.05$ in Fig. 5.2a). The random discrepancies are thought to be due to numerical error in the finite element model. In principle, these could

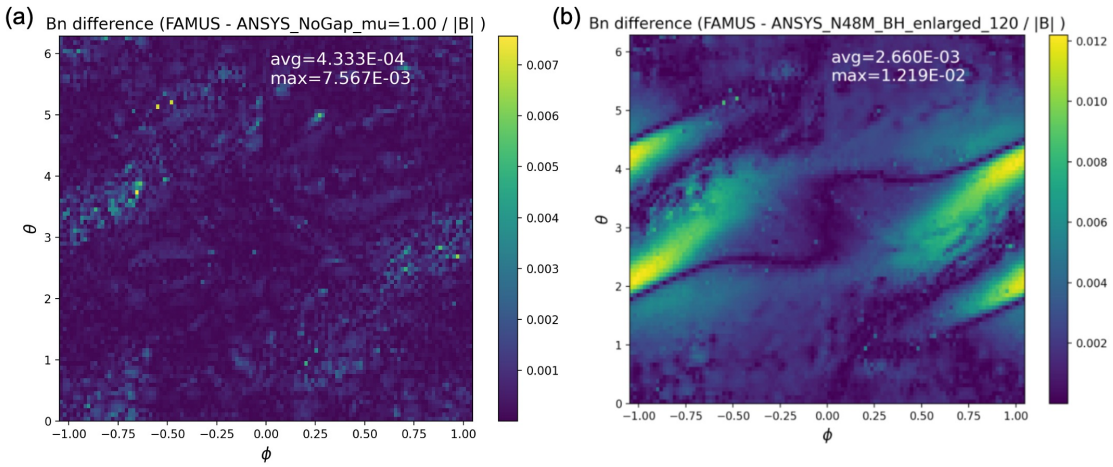

Figure 5.3: Comparisons between the calculations of the magnetic field at test points on the plasma boundary using the dipole approximation (with FAMUS) and with the Ansys Maxwell finite element model of the magnet array. These calculations use models for a full stellarator's worth of magnets including TF coils. (a) Difference between the FAMUS result and the Ansys Maxwell result with the assumption of $\mu_r = 1$ for each magnet; (b) Difference between the FAMUS result and the Ansys Maxwell result in which a nonlinear B-H curve is used for the magnet material.

be reduced through further iterations of the model; however, this was not feasible with the computational resources we had available within the time frame of the project.

For comparison, the difference between the FAMUS calculation and the calculation by Ansys Maxwell assuming a nonlinear B-H curve for each magnet—essentially the highest-fidelity option available—is shown in Fig. 5.3b. In this case, a clear large-scale spatial structure can be seen in the discrepancy across the target plasma boundary, with average and peak values both substantially greater than those seen in the comparison with the Ansys Maxwell calculation with $\mu_r = 1$ (Fig. 5.3a). These results give us good confidence in the reliability of our Ansys Maxwell model.

Bibliography

[1] C. Zhu, K. C. Hammond, A. Rutkowski, K. Corrigan, D. Bishop, A. Brooks, P. Dugan, R. Ellis, L. Perkins, Y. Zhai, A. Chambliss, D. A. Gates, D. Steward, C. Miller, B. Lown, and R. Mercurio, "PM4STELL: a prototype permanent magnet stellarator structure", *Physics of Plasmas* **29**, 112501 (2022).

[2] K. C. Hammond, C. Zhu, T. Brown, K. Corrigan, D. A. Gates, and M. Sibilia, "Geometric concepts for stellarator permanent magnet arrays", *Nuclear Fusion* **60**, 106010 (2020).

[3] C. Zhu, K. C. Hammond, M. Zarnstorff, T. Brown, D. Gates, K. Corrigan, M. Sibilia, and E. Feibush, "Topology optimization of permanent magnets for stellarators", *Nuclear Fusion* **60**, 106002 (2020).

[4] C. Zhu, S. R. Hudson, Y. Song, and Y. Wan, "New method to design stellarator coils without the winding surface", *Nuclear Fusion* **58**, 016008 (2018).

[5] K. C. Hammond, C. Zhu, K. Corrigan, D. A. Gates, R. Lown, R. Mercurio, T. M. Qian, and M. C. Zarnstorff, "Design of an arrangement of cubic magnets for a quasi-axisymmetric stellarator experiment", *Nuclear Fusion* **62**, 126065 (2022).

[6] A. Rutkowski, K. Hammond, C. Zhu, D. A. Gates, and A. Chambliss, "A novel scheme for error field correction in permanent magnet stellarators", *Nuclear Fusion* **63**, 026027 (2023).

[7] S. P. Hirshman and J. C. Whitson, "Steepest-descent moment method for three-dimensional magnetohydrodynamic equilibria", *Physics of Fluids* **26**, 3553 (1983).

[8] S. P. Hirshman, W. I. van Rij, and P. Merkel, "Three-dimensional free boundary calculations using a spectral Green's function method", *Computer Physics Communications* **43**, 143 (1986).

[9] Arnold Magnetic Technologies, *Data sheet: N48M sintered neodynium-iron-boron magnets*, `https://www.arnoldmagnetics.com/wp-content/uploads/2017/11/N48M-151021.pdf`.

[10] A. Smith, K. K. Nielsen, D. V. Christensen, C. R. H. Bahl, R. Bjørk, and J. Hattel, "The demagnetizing field of a nonuniform rectangular prism", *Journal of Applied Physics* **107**, 103910 (2010).

[11] R. Bjørk, S. Pollok, and K. K. Nielsen, *MagTense: a micromagnetism and magnetostatic framework*, `https://doi.org/10.11581/DTU:00000071`.

[12] Senis AG, *Data sheet: F3A magnetic field transducers*, `https://gmw.com/wp-content/uploads/2019/08/F3A-Magnetic-Transducer-Datasheet_rev.07.pdf` (visited on 03/09/2023).

[13] M. Landreman, "An improved current potential method for fast computation of stellarator coil shapes", *Nuclear Fusion* **57**, 046003 (2017).

[14] K. Halbach, "Design of permanent multipole magnets with oriented rare Earth cobalt material", *Nuclear Instruments and Methods* **169**, 1 (1980).

[15] P. Merkel, "Solution of stellarator boundary value problems with external currents", *Nuclear Fusion* **27**, 867 (1987).

[16] P. Helander, M. Drevlak, M. Zarnstorff, and S. C. Cowley, "Stellarators with permanent magnets", *Physical Review Letters* **124**, 095001 (2020).

[17] C. Zhu, M. Zarnstorff, D. Gates, and A. Brooks, "Designing stellarators using perpendicular permanent magnets", *Nuclear Fusion* **60**, 076016 (2020).

[18] M. Landreman and C. Zhu, "Calculation of permanent magnet arrangements for stellarators: a linear least-squares method", *Plasma Physics and Controlled Fusion* **63**, 035001 (2021).

[19] T. Qian, M. Zarnstorff, D. Bishop, A. Chambliss, A. Dominguez, C. Pagano, D. Patch, and C. Zhu, "Simpler optimized stellarators using permanent magnets", *Nuclear Fusion* **62**, 084001 (2022).

[20] A. A. Kaptanoglu, T. Qian, F. Wechsung, and M. Landreman, "Permanent magnet optimization for stellarators as sparse regression", *Physical Review Applied* **18**, 044006 (2022).

[21] *Ansys Maxwell: Low Frequency EM Field Simulation*, `https://www.ansys.com/products/electronics/ansys-maxwell` (visited on 03/23/2023).